DIRECT FORCE MEASUREMENTS OF SPECIFIC AND NON-SPECIFIC INTERACTIONS BETWEEN A SINGLE BACTERIUM AND SUBSTRATE

By

JONAH DAVID KLEIN

A DISSERTATION PRESENTED TO THE GRADUATE SCHOOL
OF THE UNIVERSITY OF FLORIDA IN PARTIAL FULFILLMENT
OF THE REQUIREMENTS FOR THE DEGREE OF
DOCTOR OF PHILOSOPHY

UNIVERSITY OF FLORIDA

2002

Copyright 2002

by

Jonah D. Klein

This work is dedicated to my parents, who continue to serve as inspirations to me; and to my loving companion, Monica, whose show of encouragement and assurance made this work possible.

ACKNOWLEDGEMENTS

First and foremost I would like to acknowledge the support of my advisor, Dr. Richard Dickinson, who has been a steady guide throughout my thesis work. Dr. Dickinson has consistently exemplified motivation, dedication, and integrity throughout my budding career in scientific research.

I also acknowledge the support of my fellow students within Dr. Dickinson's research group, particularly Aaron Clapp, who taught me the hands on fundamentals of optical trapping and evanescent wave light scattering, and Brian Burgess who introduced me to the finer details of automated light microscopy. I also acknowledge the efforts of three undergraduate students, Jennifer Vella, Ifadema Ofoma, and Seung Sung, who assisted with various laboratory measurements and duties.

For developing and supplying the bacterial mutants used in the measurement experiments, I acknowledge Dr. Timothy Foster and Dr. Orla Hartford from Trinity College in Dublin, Ireland. For helpful discussions and synthesis of polypeptides, I acknowledge Alfred Chung of the University of Florida Interdisciplinary Center for Biotechnology Research—Protein Core. For instruction and the use of the scanning electron microscope, I acknowledge Kerry Sieben of the Research Center for Particle Science and Technology and Karen Kelley, and the UF ICBR—Electron Microscopy Core, respectively.

For financial assistance and funding, I acknowledge the National Science Foundation, the NSF Engineering Research Center for Particle Science and Technology,

the Biomedical Engineering Fellowship Program, the University of Florida Chemical Engineering Department, and especially the support of my research advisor who has always hustled to secure adequate equipment and funding support.

Finally, many thanks to Shirley Kelley, Nancy Krell, and Peggy-Jo Daugherty, Dennis Vince, and to the other staff in the Chemical Engineering Department, whose support I will never forget and whose efforts have been crucial to my success.

TABLE OF CONTENTS

page

ACKNOWLEDGEMENTS iv

ABSTRACT ix

CHAPTER

1 INTRODUCTION 1

2 MEASUREMENT AND ANALYSIS OF BACTERIAL ATTACHMENT 4

- Microbial Adhesion to Surfaces 4
- Bacterial Attachment to Biomaterials 4
- Bacterial Attachment Forces 6
- Bacterial Surface Properties 7
- Non-Specific Mechanisms of Bacterial Adhesion 8
- Specific Mechanisms of Bacterial Adhesion 13
- Measurements Relevant to Bacterial Adhesion 14
  - Quantitative Attachment Measurements 14
  - Force Measurements 17

3 THREE DIMENSIONAL OPTICAL TRAPPING WITH EVANESCENT WAVE LIGHT SCATTERING 21

- Introduction 21
- Experimental Protocol 22
- Apparatus 23
- Data Analysis and Measurement 26
  - Evanescent Wave Light Scattering 27
  - Optical Trap as Force Transducer 27
  - Calibration of Optical Trap and Determination of Equilibrium and Viscous Forces 29

4 MEASUREMENT OF NON-SPECIFIC FORCES BETWEEN BACTERIA AND GLASS 36

- Force Measurements in Low Electrolyte Conditions 36
  - Reproducibility of the Technique 37
  - Viscous Interaction Forces 38
    - Comparison to DLVO Theory 40
- Force Measurements in Physiological Conditions 42

Equilibrium Profiles between Bacteria and Glass vs. Bacteria and Adsorbed Casein 44
Direct Observation of the Attachment Process 47

5 DISCUSSION AND SOURCES OF ERROR IN NON-SPECIFIC FORCE MEASUREMENTS 52

Particle Scatter and Background Scatter 52
Surface Particle Scatter and Photomultiplier Aperture Effects 54
Evanescent Wave Light Scattering and Protein Coated Surfaces 54
Torque and Rotation due to Shape Effects 57
S. aureus vs. *Lactobacillus Rhamnosus* 57
Corruption of Separation Distance Measurement by Rotation of Oblate Ellipsoids 61

6 CONTROL OF SPECIFIC INTERACTIONS AND SELECTION OF EXPERIMENTAL SYSTEM 66

Fibrinogen-Clumping Factor Interactions 66
Preparation of Deletion Mutants to Control Stalk Length 68
Biochemical Properties of Mutants 68
Physical Properties of Mutants 70
Zeta Potential measurement 70
Substrate Preparation 73
Properties of Fibrinogen 74
Peptide Conjugation 75
Evaluation of Conjugated Substrates 77
Selection and Evaluation of Adsorbed Proteins 79
Parallel Plate Flow Cell Apparatus and Measurement 80
Measurement of the intrinsic rate constant 81
Evaluation of Bovine Serum Albumin 86
Protein adsorption 86
Parallel Plate Flow Cell operation 86
Evaluation of Human Serum Albumin, Skim Milk, Casein, and β-Casein 88

7 MEASUREMENT OF SPECIFIC INTERACTION FORCES 91

Materials and Methods 91
Kinetic Rate Attachment Measurements of Mutants with Varying Clumping Factor Length 92
Force Distance Profiles for Mutants with Varying Clumping Factor Length 94
Discussion of Results 96

8 CONCLUSIONS AND SUGGESTIONS FOR FUTURE WORK 99

Conclusions 99
Suggestions for Future Work 100

Improved Optical Trap 101
Improve Measurement of Specific Interactions of Bacteria with Coated Surfaces 102

APPENDIX 105

REFERENCES 114

BIOGRAPHICAL SKETCH 121

Abstract of Dissertation Presented to the Graduate School
of the University of Florida in Partial Fulfillment of the
Requirements for the Degree of Doctor of Philosophy

DIRECT FORCE MEASUREMENT OF THE SPECIFIC AND NON-SPECIFIC INTERACTIONS BETWEEN A SINGLE BACTERIUM AND SUBSTRATE

By

Jonah David Klein

December 2002

Chair: Richard Dickinson
Major Department: Chemical Engineering

The long-term use of implanted medical devices is impeded by bacterial infection on their surfaces. When such devices are inserted in the body, plasma proteins adsorb rapidly onto the material, providing a substrate that facilitates the binding and subsequent colonization of various microorganisms including *Staphylococcus aureus*, a common pathogen found in hospitals. The attachment of a single bacterium or small clusters of bacteria to biomaterial surfaces is the necessary and often the rate-limiting step in the pathogenesis of a device centered infection. Because microbes are present in almost every aqueous environment, adhesion to other man-made surfaces (water-purification filters, air conditioning condensers, etc.) can lead to troublesome and costly problems for a variety of industries.

An investigation of both the role of both non-specific forces (i.e., electrostatic) and specific interactions (i.e., pair-wise bond formation) in the promotion of bacterial adhesion was performed through direct force measurements. In particular, the effect of

MSCRAMM (microbial surface component recognizing adhesive matrix molecules) length on attachment kinetics was investigated. Experiments were performed to 1) measure the interaction forces involved in *S. aureus* attachment and 2) determine the kinetic rate constant of *S. aureus* to various surfaces under well-defined flow conditions. These parameters were controlled through the use of specifically engineered *S. aureus* mutants that express the membrane protein "clumping factor" (ClfA) at varying lengths extending out from the cell surface.

The measurement of interaction forces and dynamics of *S. aureus* attachment was performed using a new technique that makes the uses evanescent wave light scattering (EWLS) in conjunction with 3-dimensional optical trapping. To validate the technique, measurements were first performed in simplified systems, where bare surfaces and low electrolyte conditions allowed for direct comparisons with established theories. Further investigations of the effect of MSCRAMM length on binding forces revealed the length scales at which specific interactions can act in physiological conditions as well as the magnitude of the forces involved. The corresponding measurement of kinetic rate constants of *S. aureus* attachment to surfaces was made using a parallel-plate flow chamber with the aid of automated video-microscopy, the results of which were correlated with direct force measurements.

CHAPTER 1
INTRODUCTION

The long-term use of implanted medical devices is impeded by bacterial infection on their surfaces. When such devices are inserted in the body, plasma proteins adsorb rapidly onto the material, providing a substrate that facilitates the binding and subsequent colonization of various microorganisms including *Staphylococcus aureus*, a common pathogen found in hospitals. Since the attachment of a single bacterium or small clusters of bacteria to biomaterial surfaces is the necessary and often the rate limiting step in the pathogenesis of a device centered infection, a great deal of research has been centered on identifying the plasma proteins and corresponding bacterial membrane proteins that promote adhesion. While useful, the majority of these studies do not provide a reliable means for identifying the specific cell attachment mechanisms based solely on intrinsic cell, substrate, and suspension properties. The major barriers to elucidating these mechanisms have traditionally been 1) the lack of sophisticated and relevant models that incorporate specific chemical interactions and 2) the scarcity of controllable, well defined experimental systems to validate these models.

The first quantitative engineering studies of bacterial adhesion have attacked this problem with experiments and have modeled the problem either empirically or from a purely physical basis. The development of affordable video microscopy systems has allowed for precise measurements of attachment rates of bacteria to surfaces under well-defined flow conditions. While useful for studying specific systems, measurements of overall attachment rates are relevant for the specific apparatus and not for the general case. To predict bacterial attachment rates mechanistically, transport models incorporating longer range (10-200 nm) interaction forces between a cell and a surface have been developed. These models generally consider the bacterial cell and underlying substrate to be inert, that is, only non-specific forces such as Coulombic and van der Waal's forces, and interactions including hydrophobic and steric effects are considered. For studying cell-biomaterial systems, sophisticated thermodynamic models predicting total interaction forces based upon colloidal forces as well as specific interactions such as bond formation have been developed. However, few if any experimental techniques (i.e., AFM) are currently available to fully validate these force predictions.

Because this method is the first of its kind to directly measure the interaction forces between a single microbial cell and a planar surface, many preliminary runs were required in order to validate the reproducibility of the technique. These runs were performed in simplified systems, where the use of bare surfaces and low electrolyte conditions allowed for direct comparisons with DLVO theory. A thorough investigation of the role of specific binding (i.e., chemical interactions) in the promotion of bacterial attachment was also performed. In particular, the effect of MSCRAMM (microbial surface component recognizing adhesive matrix molecules) length on attachment kinetics was investigated. Experiments were performed to 1) measure the interaction forces involved in *S. aureus* attachment and 2) determine the kinetic rate constant of *S. aureus* to various surfaces under well-defined flow conditions. These parameters were controlled through the use of specifically engineered *S. aureus* mutants that express the membrane protein "clumping factor" (ClfA) at varying lengths extending out from the cell surface.

The measurement of interaction forces and dynamics of *S. aureus* attachment was performed using a new technique that makes the use of evanescent wave light scattering (EWLS) in conjunction with 3-dimensional optical trapping. In this technique, the 3-dimensional optical trap was used to control and probe the bacterium against the surface, while a precise measurement of separation distance was using evanescent wave light scattering. Rapid measurements of fluctuating bacterium positions allowed for direct determination of potential energy and the force of interactions as a function of separation distances.

Measurement of kinetic rate constants of *S. aureus* attachment was made using a parallel-plate flow chamber with the aid of automated video-microscopy. A defined flow field of suspended bacteria was passed over a surface containing either adsorbed fibrinogen or immobilized fibrinogen fragments. The conditions used in the flow experiments were the same as that of the interaction force experiments and results of these sets of experiments were correlated together.

CHAPTER 2
MEASUREMENT AND ANALYSIS OF BACTERIAL ATTACHMENT

Microbial Adhesion to Surfaces

All non-living surfaces in nature are subject to colonization by microorganisms. After the initial attachment of a single cell or cell clusters to a surface, the subsequent cell divisions that occur under favorable growth conditions lead to the formation of micro-colonies and complex surface systems known as biofilms, which are known to cause a wide variety of costly and potentially harmful problems in various industries. For example, biofilm growth in the process industries is responsible for increased corrosion in pipes, plugging of water filters, and the reduction of heat transfer in cooling systems. Biofilm formation is also especially relevant to water treatment and purification facilities, as the formation of biofilm layers on filtration media can contaminate municipal water supplies. In the medical industry, the colonization and film formation of microbes to medical device surfaces can be potentially life threatening, as this process generally leads to infection of the host tissue.

Bacterial Attachment to Biomaterials

Various pathogenic organisms, such as bacteria, fungi, and yeast, all of which have been shown to cause medical device related infections, are present in the hospital environment. While the majority of these infections involve ordinary bacterial colonies that are centered on common devices such as catheters and prostheses (Kri89), the progression of these infections can lead to life threatening conditions such as septicemia and endocarditis (Dou88).

Device centered infections are of great concern, particularly as outbreaks of antibiotic-resistant bacterial infections become more common (Boy93, Ste02). Since there is often no effective antibiotic for particularly invasive or resistant infections (Ste01), preventing microbial colonization on device surfaces remains an emphasis in infectious disease research. In an attempt to produce infection-resistant devices, research efforts have led to an increased understanding the relevant cellular and molecular interactions involved in the pathogenesis of device-centered infections (Gri93). Since the prolonged use of any implanted medical device is often associated with infection (Ogr02), the risk associated with long-term use has proven to be a barrier to expanded use of many novel devices.

As with biofilm formation outside the body, the infection of an implanted medical device usually begins with the attachment of a single bacterium or a small cluster of bacteria to the biomaterial surface (Dan86). Because of the favorable growth conditions that exist within the host, the subsequent cell division and colonization is relatively rapid and difficult to prevent once initial attachment has taken place (Cos99). Engineers and physicians have attempted to produce microbial resistant biomaterials that serve to either minimize attachment rates of known pathogens, such as *S. aureus,* to the device surface, or develop materials that prevent their division (Her90). These endeavors are complicated by the fact that implanted devices quickly acquire a coat of plasma protein upon insertion (And88) and that the specific interaction between this coat of protein and bacterial cells is difficult to quantify. In-vivo experiments using animal models and clinical studies have been used to test the resistance of biomaterials to microbial action (Dar99). While clinically valuable, they require studies that last for months at a time and generally only provide information such as the length of time before colonies are observed, and do not offer any descriptions as to how or at what rate the microorganisms attach to the surface in the first place.

Instead, in-vitro studies have been performed that serve to not only quantify the attachment rates between single cells and surfaces under physiological conditions, but also identify the relevant plasma proteins and bacterial surface proteins involved in the process (Isb02). For the problem of environmental biofilm growth, analogous experiments have been performed on more industrially relevant systems, such as measuring attachment rates of especially prevalent or harmful bacteria to marine systems under controlled conditions (Bak02). A description of the various methods used to measure attachment rates will be provided later in the chapter along with the most significant results. Finally, the potential of using direct surface force measurement to identify attachment mechanisms will be discussed.

Bacterial Attachment Forces

To better understand the mechanism of bacterial attachment as well as interpret and evaluate the results of any technique measuring bacterial adhesion, it is essential that the forces involved throughout the entire attachment process be identified and characterized. When the cell is many diameters from the surface, it has been shown that forces such as fluid flow or cell motility act over large length scales to either accelerate or impede transport of cells to the surface. The forces involved for these systems have been described extensively for both inert and motile organisms, within physiological systems as well as for experimental systems (Dic02). However, when the cell is less than one diameter away from the cell surface, forces such as Brownian motion and electrostatic interactions become relevant (Isr01). Within several nanometers of the surface, short-range interactions such as van der Waal's forces, hydrophobic effects, and specific adhesin interactions, and steric forces have a significant effect on the probability that a single bacterium will attach (Isr01). By identifying and calculating the additive forces between the cell and surface, a theoretical probability of attachment may be determined. It is necessary then to examine both the physical and biochemical properties of the bacterial cell surface and substrate that contribute to the attachment process.

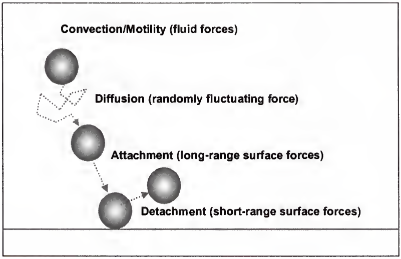
Convection/Motility (fluid forces)
Diffusion (randomly fluctuating force)
Attachment (long-range surface forces)
Detachment (short-range surface forces)

Figure 2-1. The forces relevant to microbial adhesion and the relative length scales over which they act.

Bacterial Surface Properties

Most bacterial species possess a multi-layered cell envelope consisting of a cytoplasmic membrane, a cell wall, various surface appendages, and in some cases an outer polysaccharide layer (Mad97). The inner membrane serves primarily as a permeability barrier to the environment whereas the cell wall is a rigid structure that provides mechanical support and protection from osmotic lysis. Depending upon the reaction of the cell wall with the Gram stain, bacteria are categorized into two groups, Gram-negative and Gram-positive (Figure 2-2). Gram-positive bacteria, while lacking an outer membrane, have a relatively thick cell wall consisting of mainly of peptidoglycan, a rigid polysaccharide that is sparsely interspersed with lipoproteins and other polysaccharides. Gram-negative cells possess outer walls that contain relatively little peptidoglycan but contain an outer membrane composed of packed lipopolysaccharides, lipoproteins, and other complex macromolecules. These molecules can often negative charges do to the presence of phosphate and carboxylate groups. As a result, bacterial species typically carry a net negative charge with an isolectric point in the region of pH 3 (Har53). Because bacterial cells generally exist in aqueous environments, factors such as hydrogen bonding and surface hydrophobicity become relevant when considering bacterial attachment. In addition to cell wall proteins, many bacteria possess extra-cellular structures, such as pili, fimbriae, and flagellae that allow the cells to interact more extensively than those cells with just a simple envelope structure.

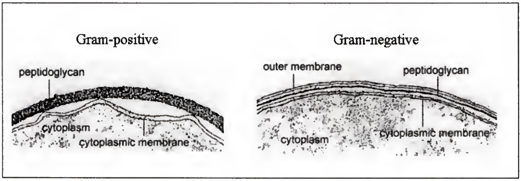

Figure 2-2. Electron micrographs of the cell of walls of Gram-positive and Gram-negative bacteria. Images used with permission. Copyright © Gary E. Kaiser

Non-Specific Mechanisms of Bacterial Adhesion

While cell-surface interactions can be mediated by specific molecular interactions, longer-range physical effects such as mechanical or electrostatic forces or thermodynamic effects such as entropic interactions are always present and must always be considered. This is especially true when considering microbial adhesion in process engineering and water purification applications. As micron sized bacteria are sufficiently small to feel the effects of Brownian motion, the first predictive attachment models were borrowed from colloid physics. Classical DLVO theory is still the most cited major theory used to quantify the non-specific long-range interactions between bacterial cells and surfaces (Her99). According to the theory, the net interaction between two surfaces can be described as a summation of electrostatic potential, $V_{R,}$ and van der Waal's potential, V_A.

$$V_{TOT} = V_R + V_A \tag{2-1}$$

The double layer potential V_R, is caused by Coulomb interactions between charged molecules. The strength and range of the force are affected by the presence and concentration distribution of the surrounding electrolytes. Charged molecules on each surface are balanced by oppositely charged ions occupying a thin region called the Stern layer. Beyond this region, accumulated counter ions and depleted co-ions exist together, the concentrations of which decay to reach that of the bulk concentration with increasing distance from the surface. When two similarly charged surfaces approach each other, the double layers interact, creating a net repelling force, V_R. A description of double layer force is given by a Hogg-Healey-Fuerstenau expression adapted for a sphere plate system (Eim95) is given by equations 2-2—2-4,

$$V_R = 2\pi a n_\infty k_B T \frac{\Phi_1^2 + \Phi_2^2}{\kappa^2}\left[\frac{2\Phi_1\Phi_2}{\Phi_1^2 + \Phi_2^2}\ln\left(\frac{1+e^{-\kappa h}}{1-e^{-\kappa h}}\right) + \ln\left(1-e^{-2\kappa h}\right)\right] \tag{2-2}$$

$$\Phi_i = \frac{ze\phi_i}{k_B T} \tag{2-3}$$

$$\kappa = \left(\frac{e^2 \sum n_{i\infty} z_i^2}{\varepsilon\varepsilon_o k_B T}\right)^{\frac{1}{2}} \quad , \tag{2-4}$$

where a is the radius of the bacterium, n_∞ is the bulk number density of ions in solution, k_B is Boltzmann's constant, T is absolute temperature, Φ_i is the reduced potential of either the plate or bacterium, ϕ_i is the surface potential of the collector or bacteria, κ is the reciprocal Debye length, e is the charge of an electron, and z is valence of an ion species. The surface potential, ϕ_i, is generally measured using electrophoresis or streaming potential measurements and generally ranges from –10 mV to –50 mV at neutral pH (van99).

Van der Waals forces result from instantaneous dipoles caused by the correlation between electrons of neighboring molecules. This interaction is always attractive and proportional to the Hamaker constant A_{132}, a material property indicative of the strength of the interaction between the two surfaces and surrounding medium. Because van der Waals forces are generally inversely proportional to separation distance, they are especially important at close range and tend to dominate the interaction at less than one nm separation. The total van der Waal's interaction for a sphere plate system was determined in (Eim95). Unlike surface potential values, the Hamaker constant, A_{132}, cannot be directly measured for bacteria and is generally estimated by applying Lifshitz theory, which requires knowledge of both the dielectric constant and refractive index of the surface components (Tru99).

$$V_A = \frac{-A_{132}}{6}\left[\frac{a}{h} + \frac{a}{h+2a} + \ln\left(\frac{h}{h+2a}\right)\right] \tag{2-5}$$

DLVO theory proposes that the total interaction potential between two surfaces is the sum of both electrostatic and van der Waal's potentials. Because both bacterial surfaces as well as most man-made materials carry negative charges in aqueous environments, electrostatic forces are generally repulsive. The length at which the electrostatic interactions act has an inverse square root dependence upon the concentration of free ions, so the range of repulsive electrostatic interactions is much longer in lower electrolyte concentrations typically found in the environment than for high electrolyte concentrations typically found within the body. Representative force distance profiles for these cases are illustrated in Figure 2-3.

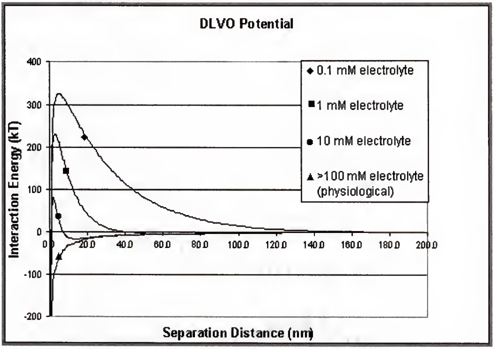

Figure 2-3. The total DLVO interaction energy is expressed as a function of separation distance (nm) for four electrolyte concentrations ($\phi_{bacteria}=\phi_{collector}=20$ mV, $A=1E\text{-}20$ J, NaCl solution).

In low electrolyte conditions, a large energy barrier (>> kT) prevents deposition due to Brownian motion alone. In physiological electrolyte conditions (>100 mM), van der Waal's attraction predominates, and bacterial deposition is expected to be transport limited.

Because DLVO theory allows for a continuous determination of interaction energy as a function of separation distance, it provides a useful conceptual framework for interpreting deposition (Mar71). However, predictions based solely in terms of DLVO often fail due to either the assumptions made in surface characterization or because other significant interactions are ignored. For example, DLVO assumes that the interacting surfaces are molecularly flat while the heterogeneous nature of the cell wall lies in contrast to this assumption. In fact, many molecular structures on the bacteria can extend beyond the interaction potential minima predicted by the theory. Furthermore, it has been postulated that correlations between reduced adhesion and negative charge may be related to the enhanced steric behavior of charged polymers as opposed to double layer repulsion.

In addition to electrostatic and steric interactions, other factors such as surface hydrophobicity has been accepted as a potential determinant of bacterial adhesion. In fact for certain bacteria-surface systems, hydrophobic interactions have been shown to predominate over DLVO predictions (Mag83). Surface hydrophobicity has been measured using hydrophobic interaction chromatography, salt aggregation, adhesion to hydrocarbon droplets, and contact angle measurements (Ach94). While good correlations between attachment rates and hydrophobicity measurements have been reported, correlations between multiple techniques are often inconsistent. In order to better account for the discrepancies between experiment and traditional DLVO theory, extensions of the model have been put forth to account for the thermodynamic change in free energy upon adhesion (van90), extended to account for hydrophobic interactions (van95), and further altered to account for polymer-induced steric forces (Juc98, Rij99).

Specific Mechanisms of Bacterial Adhesion

When considering bacterial deposition within physiological systems, the non-specific interactions mentioned above must be considered in addition to any specific molecular interaction that takes place between the cell and surface. Cells express surface associated proteins called adhesins that can bind specifically to complementary proteins expressed by the host, and the presence of these interactions can have a powerful effect on the deposition rates. Most pathogens produce MSCRAMMs (Microbial Surface Components Recognizing Adhesive Matrix Molecules), which are a sub-family of adhesins that specifically bind to extracellular matrix molecules. For example, *Staphylococcus aureus*, a gram-positive bacterium commonly found in hospitals, expresses unique MSCRAMMs that each form pair-wise bonds to the extracellular matrix proteins collagen, fibrinogen, and fibronectin, all of which are associated with infections. The specific binding of the MSCRAMM "clumping factor" to fibrinogen and its effect on bacterial deposition will be examined in more detail in subsequent chapters. This interaction will serve as the model experimental system by which the effect of MSCRAMM length and activity on interaction forces and deposition rates is evaluated.

To account for specific molecular interactions, thermodynamic equilibrium models have been constructed that model cell substrate behavior where the contact is mediated by specific binding molecules. These models require that a differentiable expression be formulated that describes the change in Gibbs free energy for the total system. The first models (Bel84, Tor86) proposed to describe mammalian cell binding and detailed a system consisting of deformable cells that progresses from a state of zero interaction to a state of total adhesion. In addition dynamic models have also been constructed that can be used to stochastically predict the attachment of both deformable cells (Lau93) as well as more rigid Brownian particles whose binding is mediated by discrete, flexible bonds (Dic97). Applying the latter model to non-motile bacteria, it was shown that very few bonds are sufficient to firmly attach a bacterium to an opposing surface because these molecules have an extremely strong affinity to their respective extra cellular proteins (Figure 2-4).

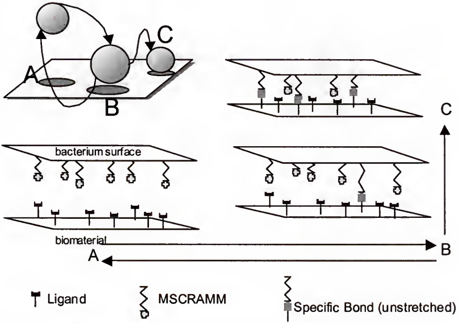

Figure 2-4—Schematic of a specific attachment process. Bacterium diffuses reversibly from free state (A) to state of close proximity (B) where binding may take place. If sufficient bonds form, the bacterium reaches an attached state (C) that is essentially irreversible

Measurements Relevant to Bacterial Adhesion

Quantitative Attachment Measurements

The affinity of cell attachment to substrates is often studied via specific batch experiments in which a concentrated suspension of cells is incubated over substrates of interest. Unattached cells are then washed off the surface and the remaining cells are counted either through radiographic labeling (Ard93), light absorption (Eim95, Sok95) or microscopic image analysis (Wit99). If a large number of cells are allowed to attach, well-designed experiments are generally useful for comparing attachment strengths of strains or substrates. However, these methods neglect to quantify the influence of fluid flow, which includes transport and wall shear rate aspects. The experimental protocols include steps such as “washing” or “rinsing” which are difficult to control or repeat. Furthermore, the results of such experiments cannot be used to accurately predict attachment rates in other flow schemes.

The advent of affordable video-microscopy systems and motorized stages has spawned the use of various flow cell apparatuses, in which the flow field of the system is carefully controlled through continuous pumping and well-defined geometries. Various configurations have been constructed that allow for the study of a host of cell properties including cell attachment, detachment, and even cell function (Fra96). Measuring the detachment rates of cells is relatively straightforward; attached cells on a microscope slide are exposed to a shear field and the number remaining is counted as a function of time. Flow cell experiments have been used to measure detachment rate coefficients for non-specific systems and systems dominated by specific binding (Bar99). In this study, a known concentration of erythrocytes was passed over a substrate and the cell density (number of cells attached per unit area) is calculated from various flow fields.

To evaluate the propensity of cell deposition, cell attachment rate constants are measured using parallel plate flow cells in conjunction with automated video microscopy systems, which measure the changes in surface concentration of cells as a function of time (Sjo90, Mei94). Assuming a uniform concentration of cells in the medium and applying first order attachment kinetics, the overall attachment rate constant k_{eff} can be determined from equation (2-6)

$$\frac{dc_s}{dt} = k_{eff} c_b \tag{2-6}$$

where c_b is the density of cells in the bulk and dc_s/dt is the rate of increase of cell surface density. Each of these parameters is a measured quantity.

Because flow chambers control the shear rate of fluid throughout the entire attachment process, the convective-diffusive transport of cells to the surface is much easier to reproduce than common batch measurements, and effective rate constant measurements k_{eff} are very reproducible. However, the transport of cells to the surface is still enhanced by higher shear rates because larger number cells are brought into close contact with the surface. If the cell adhesion is particularly rapid or slow with the respect to transport to the surface, a depletion or accumulation of cells near the surface may occur. Without a near-constant concentration of cells at the surface, an intrinsic measurement of attachment probability that is independent of transport effects cannot be determined. In order to isolate the effect of cell transport from cell-surface interactions, convective-diffusive modeling has been to estimate the actual concentration of cells able to interact with the surface. This model was first applied to a radial flow chamber (Dic95a) and was then adapted to a rectangular, parallel plate system (Rut98).

The parallel plate system was the primary method used in this study and details of the experimental procedure, model, and the results will be described in Chapters 6 and 7. By forcing a large numbers of cells in close proximity to a substrate, adhesion experiments have presented a reliable means of testing the "adhesiveness" of particular cell-surface system. Potential deposition mechanisms (hydrophobic interactions, steric interactions, specific binding) can be identified, so long as the potential competing interactions are carefully controlled and accounted for.

Force Measurements

While adhesion experiments may be useful in identifying deposition mechanisms, these techniques provide neither a means for precise control over particle positions nor a direct measurement of the surface forces acting on the particle. If the surface force between a single particle and surface can be accurately measured as a function of position, both the non-specific and specific mechanisms of bacterial deposition could be elucidated and evaluated. This task is challenging as the scale of the force necessary to attract or repel a Brownian particle to a surface is equal to the thermal energy, kT (k is Boltzmann's constant and T is absolute temperature), over the distance over which the force is applied.

When speaking of non-specific deposition mechanisms, direct surface force measurement has proven to be a valuable tool in validating DLVO theory for ideal macroscopic and various microscopic systems (Isr76, Pri90, Duc91). Furthermore, advances in atomic force microscopy (AFM) cantilever modifications have allowed for detailed investigations of short-range polymer and protein interactions and membrane mechanical properties where DLVO cannot completely describe the interactions forces (But95, Eng00). Because of the sensitivity requirements of the measurement as well as the small sizes involved, direct force measurement between whole bacterial cells and surfaces has been somewhat limited even with Atomic Force Microscopy, where the deflection of a calibrated Hookean cantilever is used to force measurement tool.

Since the AFM cantilever is significantly larger than a single cell, it is difficult to delineate the force on a single bacterium using conventional AFM. However by specially preparing a bed or lawn of bacteria, the interactions between an AFM tip and immobilized cells have been measured (van00). While most mounting procedures destroy cell viability, recent advances in substrate preparation and tip construction have preserved cell viability while significantly reducing interaction area between the tip and cell (Yao02). But since the contact between the cantilever tip and cell wall is dependent on the specific cantilever and cell properties, a detailed tip interaction model is required to obtain meaningful force distance data.

Alternatively, force distance measurements between bacteria and flat surfaces have been obtained by first mounting one or more cells to an AFM tip using a chemical fixative and probing the immobilized cell against the surface (Raz98, Ong99). While this method succeeds in simplifying the interaction geometry between the cell and surface, the mounting procedure is thought to introduce other complications such as loss of cell shape and viability. The sensitivity of the AFM methods is limited by the stiffness of the cantilever chosen. Commercially available AFM cantilevers yield sensitivities on the order of 50 pN, while specially prepared tips yield sensitivities on the order of 10 pN (Via99). Thus AFM measurements between cells and surfaces require physical contact between the tip and cell surface, which means that only short-range forces are measurable.

To measure the effect of specific interactions on cell bodies, techniques including AFM have been employed on whole cells to measure the force of adhesin interactions. For example, the molecular interactions between the ligand (RGD) and human platelet $\alpha_2\beta_3$ system was investigated by probing human platelets with AFM tips modified with RGD peptides (Lee01). However, the stiffness of the AFM tip inherently restricted the measurements in such a way that only detachment or debonding forces were recorded. In addition, the strength of extracellular adhesin, antibody-antigen, and other biomolecular interactions has been measured using a variety of novel techniques. For example, a biomembrane force probes have been developed using pressurized membrane capsules controlled by micropipette section to examine the energy landscapes of avidin-biotin binding (Mer99) or antibody-antigen binding, where antigens expressed on cell transfectants are brought into close contact with blood cells coated with corresponding antibodies (Che98). These techniques use vacuum pressure as a force transducer in conjunction with sophisticated image analysis techniques to measure cell separation and compression distances.

As an alternative to these techniques (AFM and others), it has been shown that a low power (100 mW) three-dimensional gradient optical can be used to measure force-distance profiles for micron sized silica spheres (Cla01). To date, measured force distance profiles in low electrolyte solutions have agreed somewhat well with DLVO theory for a range of particle sizes and materials. For this project, the technique of (Cla01) has been modified slightly so that the direct measurement of surface forces between viable bacteria and surfaces is possible. While other experimental techniques involving laser trapping have been recently developed to investigate the forces associated with specific biomolecular binding for model systems, no reported technique has been successful in measuring the effect on MSCRAMM binding using whole bacterial cells. The principles behind this modified technique will be the focus of the next chapter, and the significant experimental results using this method will form the basis of the dissertation.

CHAPTER 3
THREE DIMENSIONAL OPTICAL TRAPPING WITH EVANESCENT WAVE LIGHT SCATTERING

Introduction

As mentioned in the previous chapter, the optical trapping technique used to measure force-distance profiles for micron-sized silica spheres was modified for use with viable bacterial cells. When trapped, a particle of higher refractive index than the surrounding medium experiences a nearly linear restoring force for small axial displacements from the trap center (Fri96). Because the axial trap stiffness imposed on a micron-sized particle is one to two orders smaller than the stiffness of an AFM cantilever, equilibrium forces as small as 0.01 pN can be measured using a an optical trapping method (Cla01). In addition to equilibrium forces, the hydrodynamic drag force of the particle can be simultaneously measured as a function of separation distance. Since optical trapping in the near infrared has been demonstrated to have little effect on the viability of the bacterial cells at laser outputs less than 200 mW (Eri00), this technique is an ideal method for noninvasive measurements of both the DLVO-type long-range interactions involved in bacterial attachment process, as well as the steric interactions that occur during cell surface contact. In this chapter, the optical trapping apparatus, experimental protocol, and the scientific fundamentals pertaining to data analysis will be discussed.

Experimental Protocol

Various strains of bacteria were maintained as colonies on agar plates (Beckton Dickinson and Company, Sparks, MA) prior to cell harvesting. Cells were transferred from a single colony to trypticase soy broth (TSB) or other growth media (Beckton Dickinson and Company) and allowed to grow for 15 hrs at 37 °C to a concentration of ~ 5×10^7 cells/mL. One day prior to experiments, NaCl or KCl solutions (Fisher Scientific, Pittsburgh, PA) were prepared using ultra-filtered (18.2 MΩ cm) water (Barnstead International, Dubuque, IA). The suspension was then centrifuged for 15 minutes at 450 g to separate the cells and the supernatant was decanted via pipette. An equal volume of either 1mM NaCl or Dulbecco's Phosphate Buffered Saline (PBS) solution (Life Technologies, Grand Island, NY) was then added to the pellet and the solution was resuspended with a touch mixer (Fisher Scientific). The centrifugation and washing process was then repeated twice to ensure adequate separation and washing of whole cells. This resulting stock suspension was lightly sonicated for 20 minutes (Cole-Palmer Instrument Company, Vernon Hills, IL) to break up large, weakly bound aggregates. The bacteria suspension was further diluted with 1-mM NaCl to a final concentration of ~ 1×10^5 particles/mL and were supplemented w with 10 μm polystyrene spacer beads (Polysciences, Inc., Warrington, PA) to a concentration of ~1×10^4 beads/mL.

A sample chamber was prepared using treated borosilicate microscope slides (Fisher Sciences), untreated cover slides (Fisher Sciences), and bacteria/bead suspension. The microscope slides were treated overnight in Chromerge (Fisher Sciences) cleaning solution and rinsed repeatedly in ultra filtered water. The slides were further rinsed in acetone (Sigma-Aldrich Corporation, St. Louis, MO) and allowed to air dry.

A single drop of bacteria/bead suspension was placed on the microscope slide, and an untreated cover slip was placed over the drop and gently pressed downward until the 10 μm polystyrene beads were in contact with both surfaces. Excess solution was then removed using bibulous paper and the edges around the cover slide were then sealed with laboratory vacuum grease. For measurements performed in high electrolyte conditions (> 10 mM), the depletion of cells within the chamber due to attachment to the cover slip and microscope slide surfaces would be so rapid that localization and trapping would be impossible using ordinary sample preparation methods. Therefore a small suspension chamber was created by precision drilling a 0.5 cm radius × 0.5 mm deep well into the center of the microscope slide using a diamond drill bit. For these experiments, a single bacterium was selected from the well, and dragged laterally to a position underneath the prism where scattered light from the well was negligible.

Apparatus

The force measurement apparatus and procedure have been described in detail (Cla01) and are briefly summarized here. A Nikon TE300 inverted microscope (Nikon Corporation, Japan) houses a single-beam gradient optical trap (Cell Robotics LaserTweezers 100, Cell Robotics International, Albuquerque, NM) in the epifluorescence port (Figure 1). The trap was formed by a Nikon 100× objective (plan fluor, 1.3 NA) that serves to focus the 100-mW laser to a diffraction-limited spot. The sample chamber was optically coupled to the objective lens using index matching immersion oil (Cargille Laboratories, Cedar Grove NJ). The chamber rested on a computer-controlled three-axis motorized stage (Ludl Electronic Products, Hawthorne, NY) that was used to trap and localize single particles. Images were captured with a charge-coupled device camera (CCD) and viewed on a dedicated monitor.

A 45° dove prism (Melles Griot, Irvine CA) was optically coupled to the top of the sample chamber. With the aid of a rotation stage, a 17 mM He-Ne laser was directed through the prism to generate an evanescent wave. Trapped particles near the microscope slide surface scattered light that was detected by a side mounted photomultiplier tube (PMT, Oriel Instruments, Stratford, CT). The PMT signal was sent to a current preamplifier that houses an RC filter (τ_f = 150 μs). A data acquisition board (National Instruments Corporation, Austin, TX) sampled the voltage readings and wrote the results to a PC data file.

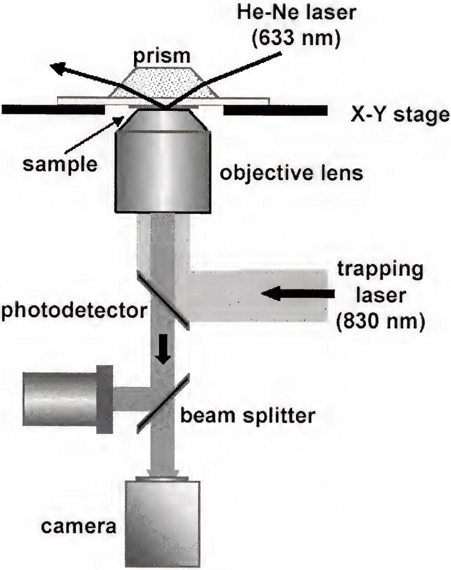

Figure 3-1. Schematic of measurement apparatus.

A Nikon TE300 inverted microscope houses a single-beam gradient optical trap in the epifluorescence port. The sample chamber rests on a computer-controlled three-axis motorized stage that was used to trap and localize single particles. Images were captured with a charge-coupled device camera (CCD) and viewed on a dedicated monitor. A 45° dove prism was optically coupled to the top of the sample chamber. With the aid of a rotation stage, a 17 mM He-Ne laser was directed through a 45° dove prism to generate an evanescent wave. Trapped particles near the microscope slide surface scattered light that was detected by a side mounted photomultiplier (PMT) tube. The PMT signal was sent through a current preamplifier to a data acquisition board that sampled the voltage readings and wrote the results to a PC data file.

With the suspension chamber in place, the motorized stage was moved manually to trap and move a single bacterium near to the microscope slide so that the scattered intensity could be observation on the dedicated monitor and maximized visually, and this maximum intensity was recorded. The bacterium was then moved to a distance from the microscope slide surface where only background levels of intensity were measurable. The configuration of the EWLS system (e.g., mirror angle, PMT aperture position) was adjusted until the level of background intensity noise was small relative to that of the maximized signal. A LabVIEW program (National Instruments, Austin, TX) was then used to step the particle toward the surface in 20 nm increments. For each motor position, the program acquired 65536 intensity samples at a rate of 20 kHz and recorded the results to a single data file. This process was repeated until the particle was as near to the surface as possible. Before any subsequent analysis, the background voltage (measured with the particle far outside the evanescent wave) was subtracted from the voltage signals.

Data Analysis and Measurement

As mentioned previously, the technique described is performed and analyzed in a manner analogously to AFM with two important differences. First, an optical trap as opposed to a rigid cantilever is used as the force transducer. Second, particle separation distances are determined by measuring the light scattered by the particle as it approaches an evanescent wave.

Evanescent Wave Light Scattering

Internal reflection occurs when light is incident from an optically dense medium at a plane interface, the other side of which is an optically less dense medium. Snell's law relates the angles of incidence and refraction. A critical angle of incidence exists where the refracted ray is parallel to the interface. If the angle of incidence is further increased, Snell's law gives a complex angle of refraction. Instead of the sinusoidal dependence on z, which is characteristic of a propagating wave, the electric field now decays exponentially with z. Because there is no real flow of energy perpendicular to the surface, this solution of the wave equation is called an evanescent wave.

The scatter intensity, I, of a spherical particle at relative position z in the evanescent wave is given by (Che79, Pri93),

$$I = I_0 e^{-\beta z} \tag{3-1}$$

where β is the inverse penetration depth and I_0 is the (hypothetical) intensity at the arbitrary origin, z = 0.

Optical Trap as Force Transducer

The linear trapping force may be described as

$$F_{trap}(z) = -\gamma_z (z - z_0) \tag{3-2}$$

where γ_z is the axial trap stiffness, z_0 is the trap center. This linear force-distance relationship corresponds to a Gaussian stationary distribution for z, with mean at z_0 and variance given by

$$\sigma_z{}^2 = \frac{kT}{\gamma_z} \tag{3-3}$$

Also, the stationary autocorrelation function of $I(t)$,

$G_I(\tau) \equiv \langle (I(t+\tau) - \langle I \rangle)(I(t) - \langle I \rangle) \rangle / \langle I \rangle^2$ is given by (Cla01)

$$G_I(\tau) = \exp(\beta^2 \sigma_z{}^2 e^{-D|\tau|/\sigma_z{}^2}) - 1 \tag{3-4}$$

where D is the particle diffusivity at the trap center. However, because the RC filter acts on the noisy signal, the actual autocorrelation function measured by the system can be approximated by

$$G_f(\tau) = C_I(\tau) + \varepsilon^2 \beta^2 \sigma_z{}^2 e^{-D|\tau|/\sigma_z{}^2} \exp(\beta^2 \sigma_z{}^2 e^{-D|\tau|/\sigma_z{}^2})(1 + \beta^2 \sigma_z{}^2 e^{-D|\tau|/\sigma_z{}^2}) + \eta e^{-|\tau|/\tau_f} \tag{3-5}$$

where $\varepsilon \equiv \tau_f D/\sigma_z^2$ is the ratio of the filter time constant, $\tau_f = 0.150$ ms, to the relaxation time of particle fluctuations, σ_z^2/D, and the parameter η reflects the added signal variance due to the (filtered) shot noise (Cla01). Equation 3-5 is precise to $O(\varepsilon^2)$.

To calibrate I_0 and γ_z for subsequent force measurements, the intensity time series was analyzed at several of trap positions located far from the range of surface forces. At each position, $\sigma_z{}^2$ was estimated performing a three-parameter fit of equation 3-5 to the measured autocorrelation function with $\sigma_z{}^2$, D, and η as fitted parameters. The trap stiffness was then calculated directly from equation 3-3 using the weighted average of $\sigma_z{}^2$, with each sample weighted by the inverse of its squared standard error when calculating the average. Also, because of equation 3-1, I is lognormally distributed with $\langle I \rangle = I_0 e^{-\beta z_0 + \beta^2 \sigma_z^2 / 2}$ when the distribution of z is Gaussian; therefore, I_0 could be estimated by the geometric mean of $< I > e^{\beta z_0 - \beta^2 \sigma_z^2 / 2}$ for the several calibration positions, z_0 (Cla01).

With I_0 and γ_z in hand, the equilibrium force on the particle at positions near the surface could be calculated from the deflection of the most-probable particle position z_p from the trap center. Since z is monotonic with I, their distributions share extrema, allowing z_p to be calculated from $z_p = -\beta^{-1} \ln(I_p / I_0)$, where I_p is the measured mode of the intensity distribution. Because z_p is the minimum of the potential energy, it is the position where the trap and the surface force balance, i.e., $F(z_p) = -\gamma_z (z_p - z_0)$.

The viscous drag coefficient δ was simultaneously determined at each position by analyzing the intensity fluctuations to determine D then applying Stokes-Einstein equation, $\delta = kT/D$. Even when the potential-energy well created by the combination of the trapping and surface forces was not strictly parabolic, equation 3-5 could still be used to estimate the diffusivity at z_p when the energy well is slightly skewed (Cla01), which was typically the case for most trap positions (the exception being regions of relatively strong attraction). Following the measurement of the drag-coefficient profile, the arbitrary relative-position scale could be then corrected to the absolute separation-distance scale by fitting the measured drag-coefficient profile $\delta(z)$ to a theoretical profile of a sphere of equal size (Bre61).

Calibration of Optical Trap and Determination of Equilibrium and Viscous Forces

Figure 3-2 describes the mean intensity $<I>$ from an optically trapped *S. aureus* bacterium in 1 mM NaCl as it was stepped in 20-nm increments toward a glass surface. The measurement was initiated at a trap position far from the surface, where the bacterium scattered a negligible light intensity and the only measured signal was due to an essentially constant background noise. As the bacterium entered the region where scatter was detectable the intensity increased exponentially because the absence of surface force caused the mean particle position to be equal to the trap center. This region was used to calibrate the optical trap position and stiffness (I_0 and γ_z). Finally, when the trapped bacterium was moved very close to the surface, repulsive forces began to limit its exponential increase in intensity by deflecting the bacterium from the advancing trap position. In this example, at no time was the optical trap able to overcome the double layer repulsion and force the bacterium to the surface. The inset summarizes the determination of the PMT shot noise constant as described in (Cla99) which ensures that signal noise is not mistaken for particle fluctuations. The Poisson shot-noise model predicts that the variance of intensity σ_I^2 divided by the mean intensity μ_I is equal to a constant value (Gar83). A linear least-squares regression yields this constant value and demonstrates that the shot noise model is accurate.

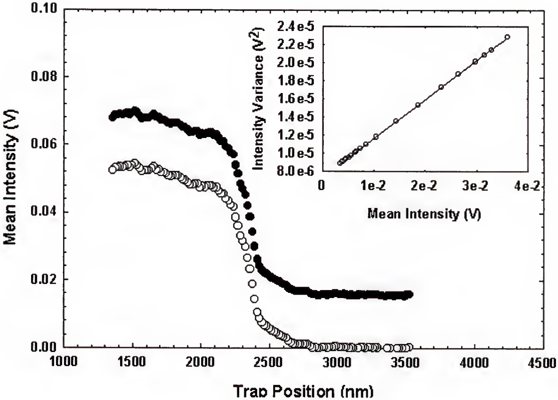

Figure 3-2. Mean of the uncorrected scattered intensity (closed circles) and background corrected intensity (open circles) vs. relative trap position.

The particle is stepped toward the surface in 20 nm increments beginning at a separation distance where particle scatter is very small relative to that of the background. As the trapped bacterium is stepped toward the surface, it begins to scatter light with exponentially increasing intensity until surface forces deflect the bacterium away from the trap center. The inset summarizes the noise calibration procedure where the square of intensity variance is plotted against mean intensity. A least square linear regression verifies that the Poisson model of PMT shot noise holds for the measurements.

At each trap position, the equilibrium force and viscous drag coefficient were estimated from the time-series of intensity samples to determine the mode, I_p, and the autocorrelation function, $G_f(\tau)$. The latter was subsequently fit to equation 5 in order to estimate the variance, σ_z^2 and the diffusivity, D. Examples of this procedure are illustrated in Figure 3-3 where the intensity autocorrelation functions and histograms of $-\beta^{-1}\ln(I/I_0)$ (which would be the corresponding particle histogram if noise were absent) are shown at two different most-probable separation distances, z_p, of 149.0 and 56.5 nm. From the fit of the autocorrelation to equation 3-5, the noise corrected position variances, the standard deviations σ_z were determined to be 27.0 and 11.5 nm, which correspond to the drag coefficients $\delta = 3.3 \times 10^{-8}$ and 4.7×10^{-8} kg / s, respectively. Gaussian distributions with means of z_p and the noise-corrected variances $\sigma_z^{\ 2}$ are also shown to illustrate the importance of noise-correction to avoid overestimation of the particle variance.

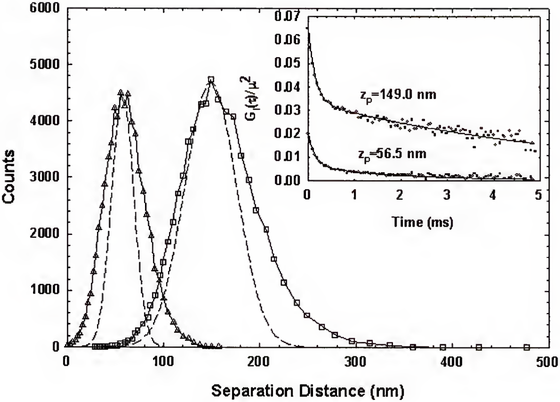

Figure 3-3. Histogram and autocorrelation function of particle positions at two trap positions.

The histogram of particle positions (open triangles, boxes) determined by $z_p = -\beta^{-1}\ln(I_p / I_0)$ is plotted along with the Gaussian distribution of positions based upon the noise corrected variance (dashed line). The intensity autocorrelation function at these positions is plotted in the inset along with the fit to the data using equation 3-5.

The trap stiffness was estimated from the weighted mean of $\sigma_z^{\,2}$ measured at multiple trap positions within the region of exponential rise in mean intensity. Figure 3-4 illustrates this estimation from the data set in Figure 3-2, where σ_z was estimated to be 29 nm, corresponding to a trap stiffness $\gamma_z = 4.8 \times 10^{-6}$ N/m.

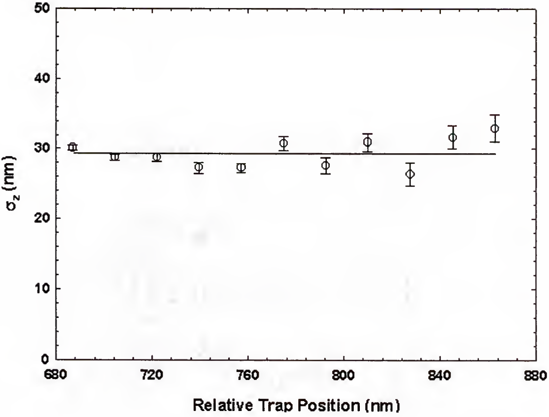

Figure 3-4. Calibration of optical trap. The standard deviation and uncertainty of particle position is plotted against trap position at a separation distance where no surface forces are present. The weighted average (black line) is used in the calculation of trap stiffness.

The figures and values detailed in Chapter 3 serve as example to show how optical trap calibration and determination of separation distances is performed for each force measurement. It should be mentioned that these steps are required each time an experimental run is made. This is primarily due to the fact that no two bacteria are identical in size and shape. Since cell size is a primary variable in determining the viscous drag coefficient, the fits of absolute separation distance to Brenner's equation do not hold from one run to another. Furthermore, subtle variances may exist with respect to optical force transduction and particle scattering that the measured trap stiffness may vary significantly from cell to cell.

In addition to detailing the measurement of non-specific forces between bacteria and glass, Chapter Four will begin with an analysis of measurement reproducibility.

CHAPTER 4

MEASUREMENT OF NON-SPECIFIC FORCES BETWEEN BACTERIA AND GLASS

Though the primary objective of the proposed project was to investigate the specific mechanisms by which bacteria attach to surfaces, the efficacy of the technique had to first be demonstrated for simple systems, where interaction forces could be easily predicted. Furthermore, measuring specific binding interactions requires the development of labor-intensive surface modifications, which are described in detail in Chapter 6. Since force measurement between whole bacterial cells and surfaces had not yet been reported in the scientific literature, a measurement system was selected that could quickly demonstrate both the reproducibility of force measurements while minimizing experimental and analytical difficulties.

Force Measurements in Low Electrolyte Conditions

Performing measurements between *S. aureus*, in low electrolyte conditions offers several advantages over other measurement systems. At low electrolyte conditions (<10 mM), the repulsive double layer interaction acting between the negatively charged cell and glass surface would be significant. This means that for a given sample, the energy barrier between the cell and glass surface makes almost every bacterium available for measurement, as electrostatic repulsive forces impede the transport of a cell to the surface by Brownian motion. In using this technique to collect data, the rate-limiting steps are the process of preparing and mounting samples, and the ability of the user to locate and trap cells within the sample. Therefore, using low electrolyte conditions and bare glass minimizes the time required to take sufficient measurements for the purposes of evaluating reproducibility and making comparisons to existing theories.

Reproducibility of the Technique

To demonstrate measurement reproducibility, samples containing *Staphylococcus aureus* were prepared using the method described in Chapter 3. After a sample was prepared and mounted, a single cell was isolated and trapped using the motorized stage. The bacterium was then probed against the bare glass surface while and trap position and particle position data was taken and analyzed. This process was repeated three times after which point both equilibrium and viscous forces were determined for the three cells as a function of separation distance. The equilibrium interaction force-profiles between *S. aureus* and glass is shown in Figure 4-1. Three experimental runs corresponding to different cells and surface locations are plotted and the corresponding semi-logarithmic plots are shown in the inset. The straight lines indicate the slope of the log of theoretical DLVO force between two surfaces in 1 mM NaCl (Debye length $\kappa = 9.6$ nm).

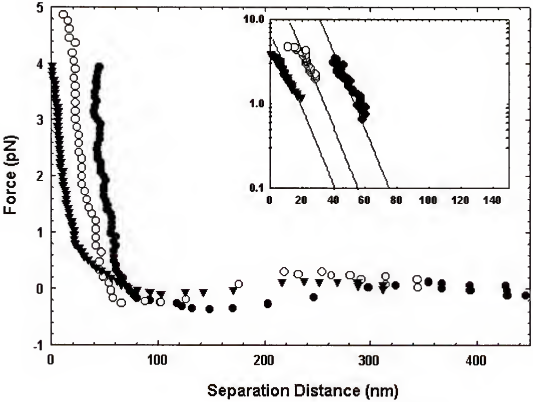

Figure 4-1. Equilibrium force measurements for three *S. aureus* bacteria near a glass plate in 1 mM NaCl.

From the plot and inset, it is apparent that the decay length of repulsive force is consistent with DLVO predictions, however, the absolute distances of each curve shows considerable variability. While the inconsistency in the measured magnitude of the forces may be partially due to variability in the cell surface potential, the uncertainty in estimating the absolute separation distance from the viscous-drag profile is likely the predominant cause of the discrepancies. Furthermore, small abnormalities in particle shape may introduce errors in extracting accurate separation distance data.

Viscous Interaction Forces

Figure 4-2 shows the dynamic interaction forces of *S. aureus* as a function of separation distance. The fractional uncertainty of the interaction force for one of the curves is shown in the inset. From this graph, it is apparent that the uncertainty in the drag calculation is highly dependent on trap position, with large uncertainty at positions where the noise is large relative to intensity fluctuations due to diffusion of the bacterium; a poor signal-to-noise ratio is encountered close to the surface where Brownian fluctuations are small in the tight balance between the surface and trapping force, and far from the surface where the scattered intensity is small. The absolute separation distance for all plots in Figure 4-2 was determined by fitting the theoretical hindered drag to the data points having the smallest fractional uncertainty where separation distance and particle radius are fitted parameters. The boxed data points correspond to those used in the fit of absolute separation distance. The fitted particle radii were found to be 400, 480, and 560 nm respectively.

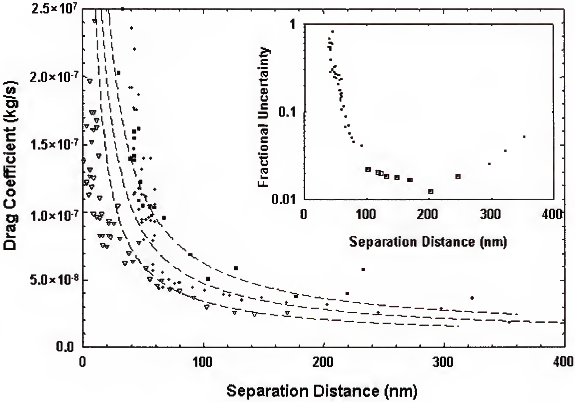

Figure 4-2. Drag coefficient measurements for three *S. aureus* bacteria near a glass plate in 1 mM NaCl.

Comparison to DLVO Theory

Because much controversy exists in the literature as to how well DLVO theory describes bacterial-surface interaction energies, experiments were performed in several electrolyte conditions to test theoretical predictions and explore potential discrepancies in measurements. For these sets of experiments, *Staphylococcus aureus* (ATTC 12600) was probed against bare glass in several solutions of potassium chloride, and the resulting interaction force was measured and compared with DLVO theory. Figure 4-3 shows the results of this study.

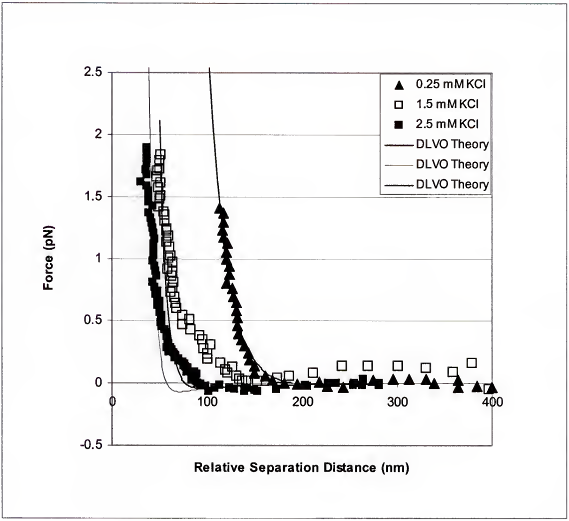

Figure 4-3. Force measurements between *S. aureus* and bare glass as a function of separation distance for three concentrations of potassium chloride.

Sample preparation and force measurements were made using methods described in Chapter 3 and the measured equilibrium force data were positioned with respect to the x-axis to best fit the calculated DLVO interactions as determined by the differentiated potential energy expressions described in Chapter 2. The Hamaker constant (A_{132}) was calculated to be 0.8 E 10-20 J from non-retarded Lifshitz theory (Tru99). The zeta potential of the bacterium as measured by electrophoresis and bare glass surface as measured by streaming potential (Tru99) was used to approximate the surface potentials of the two surfaces (-46 ± 5 mV and –44 ± 3 mV respectively).

The data corresponding to 0.25 mM KCl show excellent agreement to the theory over the range of measured separation distances, however discrepancies appear between theory and measurement at the two higher electrolyte concentrations. Though the exponential portion of the force distance profile matches well for all three concentrations of electrolyte, repulsive interactions were measured at further interaction distances than would be predicted by DLVO theory for both the 1.5 and 2.5 mM KCl measurements. One plausible explanation is that at higher electrolyte concentrations, the calculated double layers may be compressed to the point where existing surface structures on the bacterial surface may extend to the order of the double layer characteristic length. Therefore it is possible that polymer induced steric and / or electrostatic force may be predominating at smaller Debye lengths.

Due to a lack of measurements over a larger range of electrolyte concentrations and surface potentials, not to mention the fact that only one strain was analyzed, the data shown in Figure 4-3 is insufficient to settle the controversies concerning anomalous bacterial deposition data in low electrolyte systems. However these measurements represent the first time bacterial interaction forces were measured non-invasively with such low detectability. Therefore this method may prove to be a useful means of evaluating DLVO theory and others as potential descriptors of bacterial adhesion.

Force Measurements in Physiological Conditions

. In physiological or high electrolyte conditions, localization of cells within the EWLS-3DOT samples is compromised by their rapid attachment to microscope slide or cover slide surface. The sample and preparation technique had to be altered slightly to ensure that sufficient cells were available for measurement. Using a diamond-bit drill, 0.5 mm circular pits of radius 3 mm were cut into the surface of the sample slide, forming a suspension well. Figure 4-4 illustrates the sample chamber with attached well.

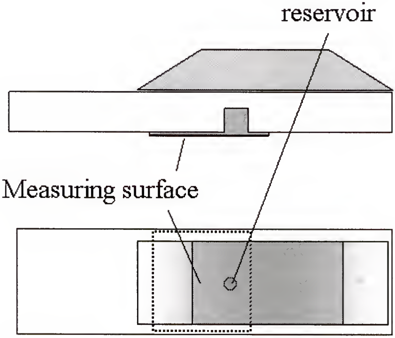

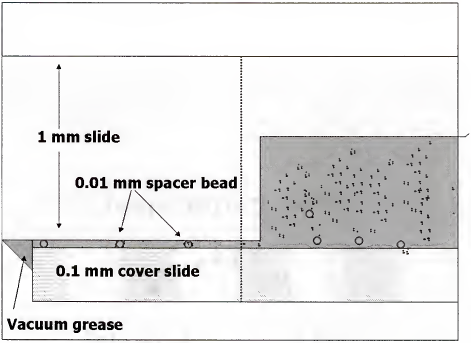

Figure 4-4 Sample modification used for measurements in attractive attachment conditions. Top view and side view are shown above (not to scale). Bacteria are trapped in the suspension reservoir (gray), and positioned into the 0.01 mm gap for force measurement.

As seen in the figure, the suspension well within the microscope slide provides a relatively deep chamber from which to localize particles. With this arrangement, particles may be trapped and within the chamber before adhesion takes place. Once a particle is trapped, it is carefully brought to a distance of approximately five microns from both the cover slide and microscope slide surface using the focus motor. Then using the stage motor, it is dragged laterally to the region where surface measurements can be made.

Equilibrium Profiles between Bacteria and Glass vs. Bacteria and Adsorbed Casein

To illustrate measurement of attractive forces as well as forces against protein-coated surfaces in physiological electrolyte, force measurements were taken using samples consisting of suspended particles in phosphate buffered saline solution (PBS).

By adsorbing a layer of β-casein on the glass, a repulsive barrier was made that would serve to completely block potential attachment sites on the bare glass.

Growth and resuspension of bacteria, and pre-cleaning of the drilled microscope slides was performed as described in Chapter 3. Following the cleaning steps, a solution of 0.10 mg / mL β-casein (Sigma-Aldrich) was prepared in PBS and filtered using a 0.22 micron Millipore syringe filter, and then added drop wise over the center of the well until a 2-4 cm^2 droplet was present. The protein was allowed to adsorb for 2 hours after which time the slide was quickly rinsed with PBS all while keeping the adsorbed protein film wet upon addition of the bacterial suspension. After sample sealing and mounting, a single bacterium was selected from the well, and dragged laterally to a position underneath the prism where scattered light from the well was negligible.

Figure 4-5 shows equilibrium force profiles for cases where a trapped bacterium was probed against both bare glass and β-casein adsorbed on glass in PBS.

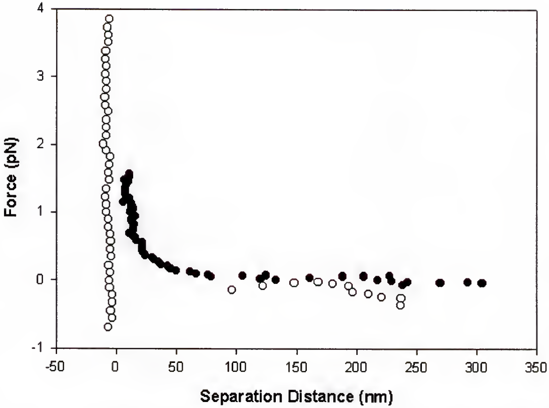

Figure 4-5. Equilibrium force measurements for a *S. aureus* bacterium near a glass plate (open circles) and near a glass plate coated with adsorbed β-casein (closed circles) in PBS buffer.

Because the total ionic strength of this solution exceeds 0.4 M, the corresponding double layer force is characterized by a Debye length $\kappa < 1$ nm, close range forces such as Van der Waals attraction and steric interactions would dominate over electrostatic repulsion typically present at low electrolytes. When the bacterium was probed against bare glass, no interaction was observed far from the surface, however, at a trap position of approximately 100 nm from the surface, attractive surface forces exceeded the restorative trapping force and the particle attachment to the bare glass was observed both visually and by particle scatter intensity, where attractive forces as great as -0.7 pN were measured. This interaction profile contrasts greatly with data taken for *S. aureus* interacting with β-casein-coated glass, where repulsive forces were observed at separation distances ranging from 10 to 60 nm.

Equilibrium force results indicate that the technique is able to resolve non-DLVO interactions in high electrolyte conditions where the bacterium appears to make physical contact with the surface. Since continuous, repulsive forces were observed for the case where the microscope slide is coated with adsorbed β-casein, whereas a discontinuous jump followed by attractive forces were observed for the bare glass system, it is likely that the casein served to sterically block the adhesion of the bacterium during the measurement. For this case, repulsive forces were first observed at a separation distance of approximately 65 nm and the minimum separation distance between the bacterium and surface was measured to be approximately 5-10 nm. This result agrees well with a previous study, where β-casein adsorbed under similar conditions was observed to occupy a steric wall of approximately 15 nm using ellipsometry in conjunction with surface force apparatus (SFA) measurements (Nyl97).

In contrast, the force distance profile of the bare glass revealed a discontinuous jump in data of approximately 100 nm to the surface, after which attractive forces were measured. The minimum separation distance (-8 nm), while not physically possible, is a reasonable result given the potential for error in estimating the absolute separation distance from the hydrodynamic drag profile.

Direct Observation of the Attachment Process

In the previous section, force distance profiles between *S. aureus* and PBS were measured under attractive electrolyte conditions, where the bacterial cell overcame the restorative force of the gradient trap and attached rapidly to the surface. Figure 4-6 represents the intensity-trap position and variance-trap position plots for such a system.

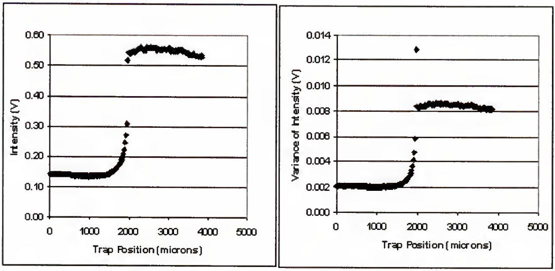

Figure 4-6 Plots of Intensity and Variance vs. Trap Position for *S. aureus* in Phosphate Buffered Saline.

From the figure it is clear that at a relative trap position of approximately 2000 nm, a large increase in particle intensity was observed between successive trap positions, indicating that the particle separation distance had decreased significantly. The considerable increase in measured variance of intensity at that point was at first so surprising that a more detailed analysis was warranted.

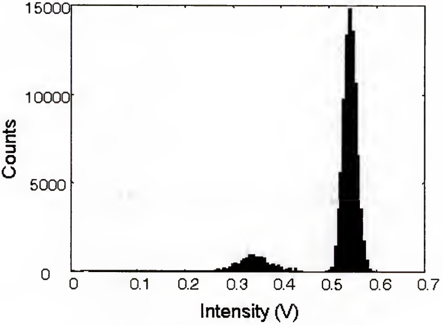

Figure 4-7. Histogram of uncorrected particle intensity for the trap position where attachment took place.

The histogram of intensities at that trap position indicates a bimodal distribution of positions (Figure 4-7). When the time series intensity data was converted to relative position as a function of time and plotted, the approach of the particle to the microscope slide could be seen (Figure 4-8).

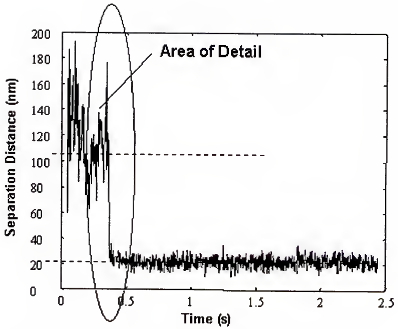

Figure 4-8. Time series data of particle attachment to surface.

Figure 4-8 represents the instantaneous particle position data sampled at 10000 Hz. The position data indicates that for approximately 0.5 seconds the fluctuating particle was held in position by the trap after which time a large fluctuation initiated a jump to the slide surface where the particle remained for the remaining 3.5 seconds. From the plot and a corresponding magnification (Figure 4-9), it is estimated that the particle moved from a trapped position approximately 80 nm over the course of 0.015 seconds, or rather, the bacterium moved at an average rate of 5 microns / second in its approach to the surface.

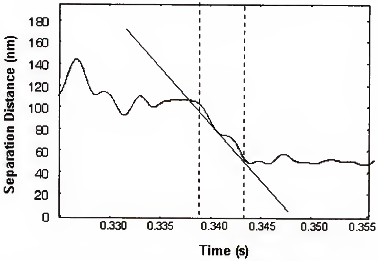

Figure 4-9. Magnification of bacterial attachment data.

Because the time required to overcome an energy barrier is thought to be the rate-limiting step in the cellular adhesion process, the subsequent rate of transport (~ 5 μm / s) to the surface shown in the figure is of lesser interest when considering adhesion. However, this result indicates that the modifications made to this measurement system allow for more detailed analyses of fundamental transport problems. Because of the high sampling rate (>10000 Hz), the trajectory of diffusing particle can be described and used to test a variety of other dynamic phenomena such as enhanced drag or electro viscous drag between a particle and surface.

CHAPTER 5
DISCUSSION AND SOURCES OF ERROR IN NON-SPECIFIC FORCE MEASUREMENTS

Combining three-dimensional optical trapping with evanescent wave light scattering presents many challenges when performing measurements between bacterial cells and surfaces. With the exception of earliest efforts (Tru99), measurements performed using evanescent wave light scattering have relied upon the use of ideal, high refractive index spheres (silica, polystyrene) and bare surfaces so that poor signal to noise ratios or shape effects are minimized. In this chapter important issues and observations leading to successful measurement between bacteria and glass as well as between bacteria and adsorbed protein will be discussed. Furthermore, the potential of error due to shape effect and torque generation is evaluated.

Particle Scatter and Background Scatter

Successful measurement of bacterial interaction force requires a strong signal from the trapped bacterium scattering light within the evanescent wave combined with a minimized amount of background-scattered light from all other objects and unwanted detections. For the system described in Figure 3-1, background detection may be caused by any and all of the following: scattering of other attached particles, unwanted detection due to poor EWLS generation, unwanted detection due to reflections, refractions of the HeNe laser within the sample, or ambient light. If the ratio of background scatter to particle scatter becomes too high, position data in the zero force region of calibration may not yield sufficient data to perform either meaningful absolute distance determinations or trap stiffness calculations. From experience, good fits of absolute separation distance to the enhanced drag coefficient may be made if the ratio of the maximum zero force signal to background signal is 3:1 or greater.

In an aqueous environment, the ability of a particle to scatter light increases with refractive index. Silica spheres of refractive index 1.4 (Geltech, Alachua, FL) scatter a significant amount of evanescent wave light. However the refractive index of bacterial cells is only slightly greater than that of water, therefore great care must be taken to minimize other background effects. Size also has a significant effect on scatter quantity in that larger cells and objects scatter light in proportion to their volume (Che79).

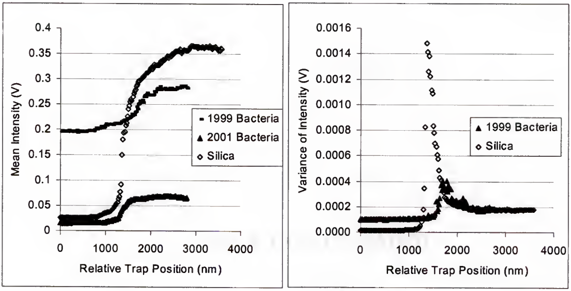

Figure 5-1. Comparison of Intensity and Variance of Intensity vs. Trap Position between Silica and *S. aureus* bacteria

Figure 5-1 compares typical force distance profiles between 1-micron silica and glass with that of *S. aureus* data taken in 1999 and with data taken more recently. From the graph it is clear that signal from the silica particle greatly exceeds that of bacteria. Comparison of the two intensity-trap position profiles for *S. aureus* indicates that improvements have been made to reduce the level of background scattering. The causes of high background signal and the steps taken to reduce it are described in the next sections.

Surface Particle Scatter and Photomultiplier Aperture Effects

Scattering of nearby particles on the microscope slide surface contributes to significantly increased background noise levels. For example, taking intensity measurements within a few microns of large neighboring particles (i.e., a spacer bead) leads to large background signals. However, particles or surface scratches very far from the objective lens may also contribute to background scatter via reflections that occur within the sample. This is evidenced by the fact that samples with more concentrated suspensions have much higher background signals than so those with dilute suspensions. Because background noise is additive, it is best to minimize scatter by keeping suspension concentrations at minimum while at the same time introducing sufficient particles to perform an experiment.

By optimizing the position and size of the photomultiplier aperture, the background signal from neighboring particles was reduced significantly. A second CCD camera was placed over the PMT port so that the size and position of the aperture in relation to the object of interest allowed only the smallest amount of background light to be detected.

Evanescent Wave Light Scattering and Protein Coated Surfaces

Performing evanescent wave light scattering with surfaces coated with adsorbed proteins or protein fragments required additional care when considering total internal reflection. In the work of Ruta 1998, parallel plate flow cell experiments involved adsorbing proteins to microscope slide surfaces. Slides were typically immersed in Petry dishes filled with concentrations of fibrinogen and other proteins including skim milk. In this scheme, both sides of the slide surface were allowed to adsorb with protein.

When this adsorption method was employed for the purpose of taking force measurements, large background signals prohibited meaningful intensity measurements and trap calibrations. In addition, transmitted images of the surfaces prepared in this manner had a dynamic, wavy appearance when total internal reflection was attempted, suggesting a significant penetration of the He-Ne beam through the glass-water interface. It was first hypothesized that this increase in signal was due to the presence of adsorbed protein scattering light at the glass water interface. However, experiments were performed where only one side of the slide was put in contact with proteins, and the protein coated slide was allowed to contact either the immersion oil or glass-water interface. Because both the waves and large background signal were only observed when the protein surface was in contact with oil, there was evidence to suggest that the protein was disrupting total internal reflection by refracting and scattering light prior to total internal reflection at the glass water interface. Because such refractions or scattering angles may be dependent on objective lens position, it is believed that proteins or any other material on the surface of the slide in contact with the immersion oil and prism will corrupt position measurements significantly. In fact, all experiments performed subsequent to this observation included an additional cleaning step of the microscope slide surface. Prior to prism mounting, the top surface of the microscope slide was wiped clean with lens cleaning solution.

In addition to aperture adjustment and greater care in sample preparation and design, the sample construction (described in Chapter 6) served to further reduce problematic scattering effects. The use of drilled slides (Figure 4-4), allowed for smaller concentrations of particles as the suspension chamber makes a large volume available from which to localize bacteria. Therefore, fewer bacteria would ultimately attach to the microscope slide surface and contribute to increased background scattering.

Second, great care was taken to maintain the cleanliness of the slide in contact with the immersion oil. When performing bacteria—protein experiments, a small liquid bead of protein was incubated on the surface of the slide, and great care was taken to ensure that this surface remained wet throughout the adsorption process. It should be mentioned that an increase in scatter was observed when adsorbed proteins were present, and this scatter increased considerably when portions of the slide surface were allowed to dry completely. It is believed that microscopic, insoluble proteins and impurities are able to adsorb the surface and scatter light to some degree. The use of syringe filters as described in Chapter 6 reduces background scatter to the point where bacteria—protein measurement is possible. Table 5-1 summarizes the approximate signal to noise ratios of several measurement systems where the signal to noise ratio is defined by the mean signal corresponding to maximum variance of intensity divided by the signal measured in the absence of particle scatter. Due to variances in particle size and sample preparation, these ratios may vary from measurement to measurement and only approximate or expected values are shown.

Torque and Rotation due to Shape Effects

One potential source of error, independent of background scatter, is the effect of shape. While it is true that bacteria such as *Staphylococcus* and *Streptococcus*

Table 5-1. Observed Signal to Noise Ratios of Selected Measurement Systems

System	Approximate Signal to Noise Ratio
Silica--Glass	25 : 1
Silica—Unfiltered Protein	15 : 1
Bacteria--Glass	4 : 1
Bacteria—Filtered Protein	3 : 1
Bacteria—Unfiltered Protein	2 : 1
Bacteria—Protein Adsorbed Both Sides	Data is Corrupt

approximate spheres, imperfections in shape may lead to error in the determination of position data. By following the analysis of both rod shaped and spherical strains, the potential for error in using non-spherical particles was assessed.

S. aureus vs. *Lactobacillus Rhamnosus*

Lactobacillus rhamnosus is a rod-shaped lactase-producing bacterium originally isolated from the intestinal tracks of humans. It was chosen for study because like *S. aureus*, it is gram positive, non-motile, does not express pili or fimbraie, and does not release spores within the measurement sample. The dimensions of *Lactobacillus rhamnosus* rods measure approximately 0.8 × 0.8 × 2.5 microns and when in the presence of an evanescent wave, these cells scatter light on the same order of magnitude as *S. aureus*.

In order to test the effect of particle shape on force measurement results, measurement samples of *Lactobacillus rhamnosus* (ATTC 7469) were prepared (as described in Chapter 3) in 1-mM NaCl. Upon sample preparation, the bacteria were localized and trapped; and as expected, trapped cells aligned perpendicularly to the microscope slide surface. Oblong particles such as rods, needles, or ellipsoids, align perpendicularly to the slide surface due to the fact that the gradient optical trap employed has a stronger stiffness coefficient in the lateral directions than it does the axial direction.

Trapped particles were stepped toward the surface in even increments and particle positions were recorded as a function of trap position and compared with *S. aureus* measurements taken in the same electrolyte concentration. Relative trap position data was adjusted in the z direction for the purpose of superimposing plots. Typical intensity-position curves for both rods and spheres are shown in Figure 5-2, where two regions of exponential increase in intensity were observed. Initially, the presence of two exponential regions presented a puzzling situation in terms of choosing potential trap calibration points.

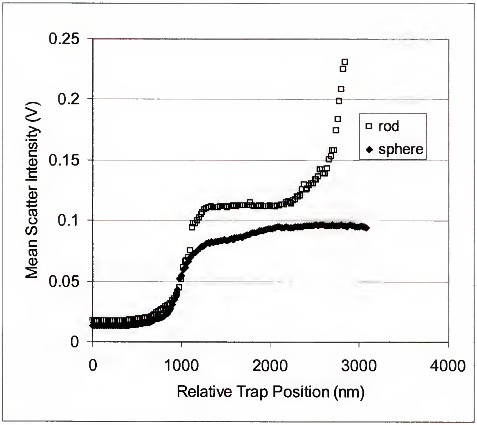

Figure 5-2 Intensity vs. Trap Position data for *Lactobacillus rhamnosus* and *S. aureus* bacteria.

At the conclusion of experimentation, the long dimension of the rod had moved from a perpendicular orientation to a parallel one and image acquisitions were taken to support this conclusion (Figure 5-2). Real time output of data allowed for the mean intensity measurements to be correlated with visual observations of particle orientation. Repeated runs indicate that the second exponential increase in mean intensity corresponded exactly with transitional rod orientations (neither parallel nor perpendicular). Therefore, trap position existed where the rotation of the rod is actuated by optical torque. It is believed that reorientation within the optical trap served to increase the mean intensity by orienting a larger fraction of the cell at smaller separation distances, where the intensity of the exponentially attenuating evanescent wave was more intense. For *Lactobacillus rhamnosus*, changes in orientation were observed at a trap focus positions beyond the range of measurement and beyond the range where the assumption of force-displacement linearity is expected to hold.

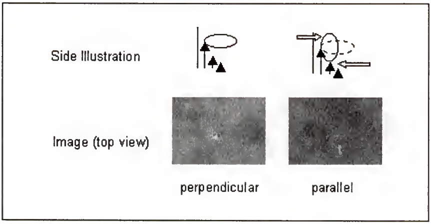

Figure 5-3. Illustration and image capture of the rotation of a rod shaped bacterium.

Data analysis and equilibrium force measurement were performed for both rod-shaped and spherical cells, the results of which are shown in Figure 5-3. The DLVO parameters chosen are identical to the ones used in Chapter 3. Because, zeta potential data for *L. ramnosus* were not taken, it was assumed to be equal to that of *S. aureus*. For the case of *L. ramnosus,* the first exponential rise in mean intensity was chosen as the trap calibration region and measurements were recorded for all trap positions prior to the observed change in orientation.

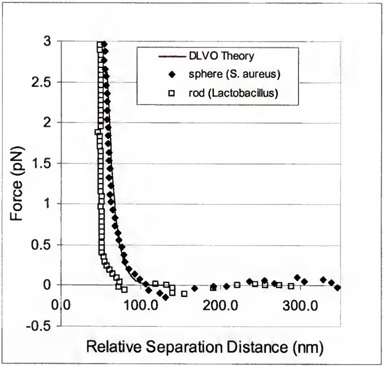

Figure 5-4. Force vs. Separation Distance for bacterial rods and spheres compared to DLVO theory.

From the plot, it is clear that equilibrium force measurements reveal distinct similarities for both rods and spheres, but the separation distance at which repulsive forces are observed is much smaller for the *L. ramnosus* strain. Furthermore, the slope of the force distance interaction is significantly steeper than for the spherical case. From this plot, it appears that the EWLS-3DOT system is capable of measuring surface forces on rod shape particles so long as care is taken in the selection of calibration and measurement regions.

Corruption of Separation Distance Measurement by Rotation of Oblate Ellipsoids

The fact that torque was generated at all for non-spherical particles indicated that some form of planar asymmetry existed within the measurement system. Repeated observations indicated the orientation of particles within the sample tended to follow similar trajectories, and that the orientation of the trapping laser may not have been completely perpendicular with respect to the plane of the microscope slide. Furthermore, the trapping and probing of higher aspect ratio particles (needle-shapes) against bare glass either did not induce reorientation until the trap focal position was several thousands of nanometers beyond the microscope slide surface.

Potential discrepancies proposed for spheres were generally observed 50 to 100 nm from the surface and are observed sporadically. It is important to remember that *S. aureus* bacteria and others *coccus* strains only approximate spheres and relative to synthesized silica, can be slightly oblate. For visual comparisons between *S. aureus* and silica, note SEM micrographs in Figure 5-5 and observe the differences between the micron sized silica sphere (Geltech, Alachua, FL) and the two slightly smaller and more oblate *S. aureus* bacteria. Refer to Chapter 6 for details of SEM micrograph preparation.

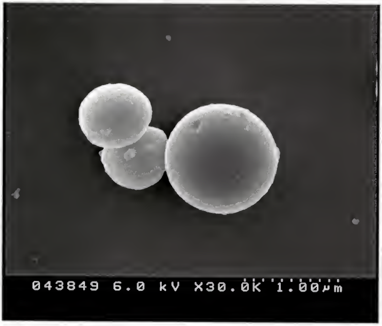

Figure 5-5. Electron micrograph of 1 μm silica and *S. aureus* bacteria

If aspect ratio is a determinant in the distance at which torque generation actuates reorientation, the following explanation is proposed to account for discrepancies between measured equilibrium forces and DLVO predictions for *S. aureus* bacteria. It is believed that for objects that approximate spheres (very small aspect ratios), torque generation and particle reorientation can occur very soon after the onset of repulsive particle displacement from the trap center. In the following experiment, an *S. aureus* bacterium (the same "spherical" particle shown in Figure 5-1) was trapped and probed against the surface. Equilibrium force-distance profiles matched closely until a separation distance of approximately 80 nm, where the particle assumed a much closer separation distance than is predicted by DLVO. While the aspect ratios and reorientations are too small to detect by visually, it is believed that at this distance, torque induced reorientation begins to reorient a larger fraction of the cell in the presence of the evanescent wave, making for smaller separation distances smaller than one would expect for the given trap position.

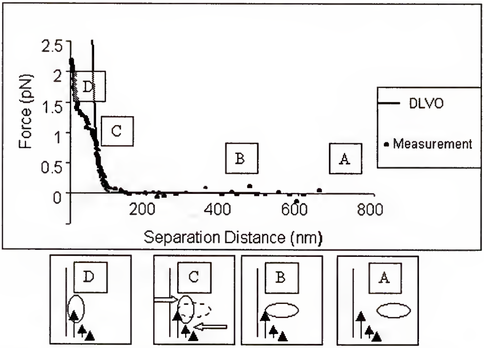

Figure 5-5. Force-distance profile between a prolate sphere and a flat surface.

This observation can also be seen in the mean-intensity separation curve shown in Figure 5-2, where close examination reveals small but significant increase in intensity at a relative trap position of approximately 1800 nm. In the corresponding force measurements, deviations from DLVO theory occurred at this exact trap position, indicating that even small asperities may have a demonstrable effect of separation distance determination. Because small aspect ratio particles reorient themselves at shorter relative trap positions, and the effect of reorientation is hard to detect, the potential for torque- induced error is an important point of consideration for all particle-plate systems.

In this chapter, potential sources of measurement error and uncertainty were examined. The first section detailed some of the modifications in data collection and sample preparation that allowed for force measurement between bacteria and glass as well as force measurements between bacteria and adsorbed protein. The identification and subsequent reduction of background detection and noise was critical in allowing successful force measurements of the specific interactions described in Chapters 6 and 7.

Beyond selecting those bacteria that appear most spherical, no successful solution was found to eliminate the effect of particle rotation on the force-distance profiles. However, it should be stated that the optical trap employed in surface force measurements was built commercially and the tools necessary to build "in-house" optical traps exists. It is believed that torque-induced reorientation was caused by a combination of asymmetry and a relatively large magnitude of lateral (x-y) gradients relative to axial gradients. By designing a trap with significantly reduced lateral gradients (on the same order of magnitude as the axial gradient), the potential effects of optical torque may reduced to less-significant levels.

CHAPTER 6
CONTROL OF SPECIFIC INTERACTIONS AND SELECTION OF EXPERIMENTAL SYSTEM

While specific adhesin-mediated interactions are extensive and are not limited to bacteria, a well-controlled system may offer insight in the analysis of more general cellular deposition processes. Advancements made by collaborators at Trinity College have allowed for a means of controlling adhesin length using viable *Staphylococcus cells*. This chapter reviews the nature of specific protein-protein interactions between the *S. aureus* surface and fibrinogen as well as some of the resulting effects on adhesion enhancement to surfaces. The steps taken in choosing a suitable experimental substrate is presented, beginning with a description and evaluation of mutant cells that were developed by our collaborators. Finally, an account of the methods taken to develop and evaluate controlled substrates for use in force and deposition measurements is presented.

Fibrinogen-Clumping Factor Interactions

S. aureus expresses a family of specific protein adhesins (microbial surface components recognizing adhesive matrix molecules, or MSCRAMMs) that mediate its adherence to the extracellular matrix components of the host (McD94, Sig89, Swi89, and Lia95). Matrix molecules are present in blood plasma and usually found adsorbed to biomaterial surfaces shortly after contact with the host. This interaction of cellular adhesins with matrix molecules has been shown to promote attachment to implanted medical devices. Examples of these matrix proteins include Protein A, fibronectin, collagen, vitronectin, and elastin, and fibrinogen. Though cellular MSCRAMMs interact uniquely with their corresponding matrix proteins, they have certain genetic and structural features in common. For example, hydrophobic amino acid residues near the C-termini anchor the protein to the cell membrane while hydrophilic N- termini allow the binding region of the protein to extend and interact with the host by binding to host proteins or cells.

S. aureus expresses an adhesin called clumping factor (ClfA), which is the cell surface protein responsible for binding to fibrinogen. This 933-residue protein has been shown to promote the attachment of bacterial cells to biomaterial surfaces immediately after contact with the host (Vau95, Vau93). Clumping factor derives its name from the fact that visible clumps of bacteria form in concentrated bacterial suspensions containing fibrinogen. By extracting ClfA protein from lysed cells, the specific interactions between dissolved *S. aureus* clumping factor (ClfA) and fibrinogen have been characterized (McD95). By passing purified clumping factor over a surface plasmon resonance sensor immobilized with fibrinogen, the dissociation rate constant of the Fg-ClfA was experimentally measured to be 0.51 ± 0.19 μM, indicating a strong interaction (McD97).

Genetic mapping and novel investigations of the *S. aureus* genome have led to the identification, manipulation and expression of the clumping factor gene. The primary structure, and corresponding orientation within the cell wall has been deduced from both its DNA sequence as well as from relative hydrophobicities of both the membrane and wall *S. aureus* (McD94). The following significant structural regions have been identified: signal sequence (S), binding domain (A), repeat domain (R), wall spanning domain (W), transmembrane domain (M), and stop sequence (++). The regions are depicted in Figure 6-1, where the numbers in parentheses indicate amino acid number.

This structure is considered to be representative of common adhesins found on the *Staphylococcal* cell wall.

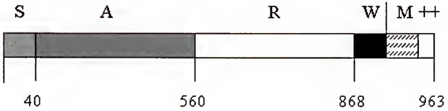

Figure 6-1. Schematic diagram of Clumping Factor Structure

The repeat region (R) of the clumping factor gene is unusual in that it is comprised exclusively of aspartate—serine (SD) dipeptide subunits (308 in all). It has been postulated that these SD repeats in region R are required to span the cell wall peptidoglycan and to act as a "stalk," allowing the ligand binding region to be displayed in an active form far from the cell wall.

Preparation of Deletion Mutants to Control Stalk Length

In order to measure what effect MSCRAMM structure has on activity or deposition enhancement, mutant strains lacking in genes or gene segments have been constructed and their corresponding interaction to proteins have been measured. For example, clumping factor-defective mutants of *S. aureus* were isolated by transposon mutagenesis (McD94). These cells failed to clump in soluble fibrinogen and adhered poorly to fibrinogen-coated cover slips. However, the introduction of a cloned ClfA gene into clumping factor deficient strains restored both clumping and adherence to adsorbed fibrinogen.

Biochemical Properties of Mutants

To test the function of the dipeptide repeat region R, deletion mutants lacking the "R" encoding region were generated (Har97) as well as variants having truncated region

R domains. Table 6-1 and the corresponding Figure 6-2 illustrate the length of region R in number of residues as well as the corresponding length in nanometers assuming that the stalk is α-helical (Rut98). For a full description of the methods used to construct, characterize, and confirm the successful control of stalk length refer to Hartford 1997.

Table 6-1 Properties of *S. aureus* Mutants

Strain	Number of Repeat	Estimated Stalk
A2	N / A	N / A
CF56	0	0
CF85	9	1.6
CF84	21	3.7
CF80	79	13.9
CF82	121	21.3
CF81	133	23.4
CF78	157	27.6
CF54	307	54.0

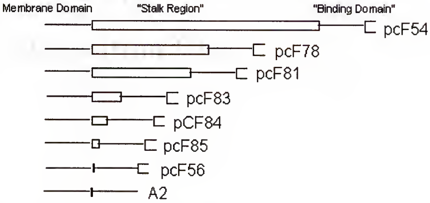

Figure 6-2. *S. aureus* mutants constructed with variable length of repeat region.

Constructed mutants were evaluated on their ability to clump in soluble fibrinogen, adhere to immobilized fibrinogen, and adhere to clumping factor antibodies. Mutants lacking region R altogether did not clump in soluble fibrinogen, and exhibited significantly lower levels of adherence to fibrinogen and anti-ClfA serum. It was found that a minimum of 72 residues between region A and the LPDTG sequence were required for wild-type levels of clumping. As the length of region R was decreased from 72 to 4 residues a decrease in clumping titre (numbers of dilutions of fibrinogen required for clumping) was observed.

Physical Properties of Mutants

Collaborators (Hartford, Foster et al.) at Trinity College, Dublin have generously provided mutant strains of varying stalk length for further study, where the interactions between whole cells and adsorbed fibrinogen can be measured using the force measurement technique previously described. While our collaborators explored biochemical interactions between mutants expressing truncated clumping factor and fibrinogen, potential physical differences resulting from genetic preparations were not explored. Because both the optical force measurement parallel plate flow techniques are physical measurements dependent on properties such as size, shape and surface morphology, these properties required some rudimentary physical characterization. With the mutant strains in hand and several characterization techniques available, properties of strains were compared using both zeta-potential and scanning electron microscope characterization methods.

Zeta Potential measurement

While electrostatic interactions are not believed to be a predominant mechanism mediating cell surface forces in physiological electrolyte conditions, the presence of specific proteins and polysaccharides have been shown to alter the surface charge of bacterial cells. The isolectric point of the clumping factor protein is not known, however, it was hypothesized that negatively charged aspartate residues on the cell surface might alter the negative charge on the cell surface. In order to test this hypothesis, zeta potential measurements for each mutant strain were made and the resulting zeta potentials were recorded.

Mutant strains were grown up overnight, washed, and resuspended in 1 mM NaCl at concentration of approximately 10^6 cells /ml. Using a Brookhaven Zeta Plus, the suspension was placed in a cuvette tube, in which an electrophoresis electrode was inserted. After an appropriate voltage was applied across the sample, the electrophoretic motility of a the particles and corresponding zeta potential was determined for several strains, the mean and uncertainty of which are shown in Figure 6-3.

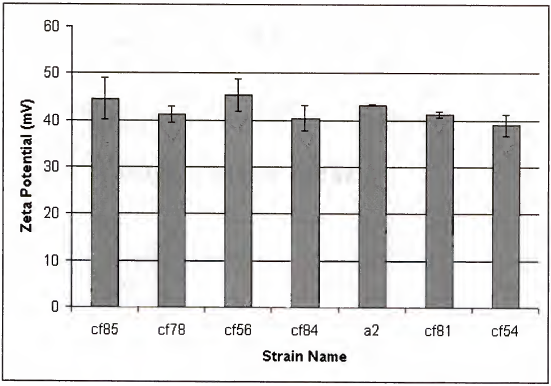

Figure 6-3. Zeta potential of clumping factor mutant strains.

The results shown in Figure 6-3 indicate that neither stalk length nor the presence of clumping factor on the cell surface has a demonstrable effect on the measured zeta potentials. In fact, the difference in mean zeta potential between strains is generally within the uncertainty of the measurement, which indicates that the presence of the clumping factor protein is not sufficient to disrupt the electrical surface properties of the cell.

Electron microscopy

The application of the force measurement technique described in Chapter 3 requires that cells used approximate spheres. However, comparisons of physical features such as shape, roughness, or size had not been made between both mutant and wild type strains thus far. Electron microscopic images were taken of wild type strains and the reconstituted mutants to determine if any physical differences could be discerned.

Cells were prepared in phosphate buffered saline and fixed in solutions of 1 % glutaraldehyde, mounted on poly-L-lysine coated glass cover slips, and further treated with 2% osmium-tetraoxide in water. To preserve cell shape and morphology, the following dehydration method was employed. Water was removed from the cells through successive washings in increasing concentrations of ethanol / water solutions until the ethanol was displaced by liquid CO_2 in a critical point dryer and allowed to evaporate slowly. Samples were sputter coated with platinum / gold mixture and images were obtained using a Hitachi S-4000 FE-SEM of maximum resolution equal to 1.5 nm. Images are shown in Figure 6-4.

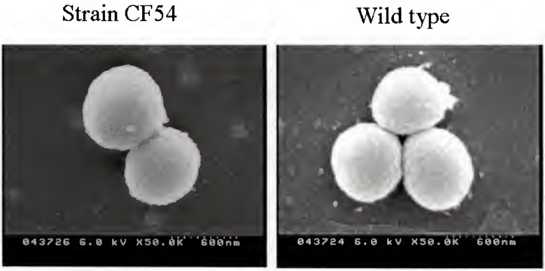

Figure 6-4. Scanning electron micrographs of cf54 and wild type *S. aureus*.

From the images, it is observed that both the wild-type *S. aureus* characterized in Chapter 3 and the mutant strain cf54 expressing clumping factor of equivalent length have physically similar properties. Both cells are roughly spherical in shape have on an average cell diameter of 730 ± 10 nm (n = 20). The surface of both cells are well defined and display a similar surface roughness, indicating that the plasmid-expressed clumping factor does not alter the physical surface morphology in any appreciable way. The cell diameter of the strains as measured by SEM was significantly smaller than the diameter as determined by the fit of the hydrodynamic drag data 940 ± 40 nm (n = 3), which indicates the likelihood of cell shrinkage during the preparation procedure.

Substrate Preparation

The interaction of clumping factor protein with fibrinogen occurs at specific sites on the fibrinogen molecule. Because fibrinogen and other plasma proteins are large relative to the estimated expressed stalk length of *S. aureus* mutants, efforts were taken develop ideal substrates that best control the interaction distances between an optically trapped cell and substrate. In this section, a description of the role of adsorption fibrinogen in mediating *S. aureus* attachment to its surface is presented followed by an account of the methods developed to display active clumping factor binding sites on the surface.

The goal was to create a well-defined substrate that can be used in both deposition rate experiments as well as optical force measurements while minimizing all interactions unrelated to specific *S. aureus* binding to fibrinogen. Microscope slides were modified using direct bio-conjugation of binding sites as well as passive adsorption methods. The first approach involved cross-linking the 12-residue clumping factor binding site directly to glass. Because this approach was unsuccessful in controlling for non-specific effects, a second approach involving the adsorption of whole proteins was developed was eventually chosen as the substrate used in surface forces and deposition rates measurement.

Properties of Fibrinogen

The plasma protein involved in promoting *S. aureus* attachment to biomaterials is fibrinogen, a soluble plasma protein that binds to specific adhesion molecules distributed across the bacterial cell membrane. While the primary physiological function of fibrinogen is to form insoluble fibrin clots (Doo84), interactions between fibrinogen and fibrin, thrombin, platelets, and especially bacteria are all relevant when considering the long-term use of medical implants.

Fibrinogen is a large (340 kDa, ~40 nm) protein made up of six dimeric polypeptide chains which when active, form three distinct structural domains called alpha, beta, and gamma subunits. The affinity of fibrinogen to *S. aureus* is extremely strong. Clumping of *S. aureus* has been observed when only 20 molecules of human fibrinogen per one staphylococcus are present (Haw82). Using radiolabeled fibrinogen, the investigators determined the binding dissociation constant for fibrinogen—clumping factor interactions to be 9.9E-9, and that approximately 2130 molecules bind for each bacterial cell. Using radiolabelled Fg fragments and corresponding monoclonal antibodies, binding assays have identified the specific region of interaction on the fibrinogen molecule to be on the last twelve residues of the gamma chain (McD95). This finding was confirmed when a synthetic 12-residue polypeptide was shown to inhibit the binding of *S. aureus* to immobilized fibrinogen.

Peptide Conjugation

Because the 12-residue polypeptide mentioned above has been shown to inhibit clumping factor-fibrinogen interactions, it was hypothesized that the same peptide could be grafted on to microscope slides to promote attachment. To test this, the peptide N-HHLGGAKQAGDV-COOH as well as a 12-residue control isomer was synthesized by the Interdisciplinary Center for Biotechnology Research—Protein Core at the University of Florida. To best mimic the binding of clumping factor to fibrinogen, this binding site was immobilized at its the amino terminus, thus exposing the carboxyl terminus to reaction with clumping factor. Because the polypeptide contains lysine (which contains an additional primary amine group), the peptide was synthesized with a protecting group (Dde) on the lysine residue, preventing its reaction during the carbodiimide reaction. The protocol, which was developed from several sources (Won93, Dee95; Olb96) is summarized below and illustrated in Figure 6-5.

Glass microscope slides (Fisher) were cleaned and etched in sodium hydroxide to maximize surface silanol (SiOH) concentrations. Reaction with aminopropyltriethoxysilane yielded primary amine groups on the surface (1) and further reaction with succinic anhydride converted the primary amines to carboxylic acid groups while introducing a four-carbon spacer (2). These acid groups reacted with N-hydroxysuccinimide in the presence of N,N' dicyclohexylcarbodiimide to make active ester intermediates (3) which were then covalently bound to the peptide at its amino terminus (4). Lysine side chains containing the protected primary amines (open circle) were then deprotected with hydrazine while unreacted esters were then passivated with glycine. Finally, adsorbed peptides were removed using solutions of urea and sodium chloride. Evidence of successful conjugation was obtained through amino acid analysis performed by the ICBR, however, the actual numbers of conjugated control and active peptides were not quantified.

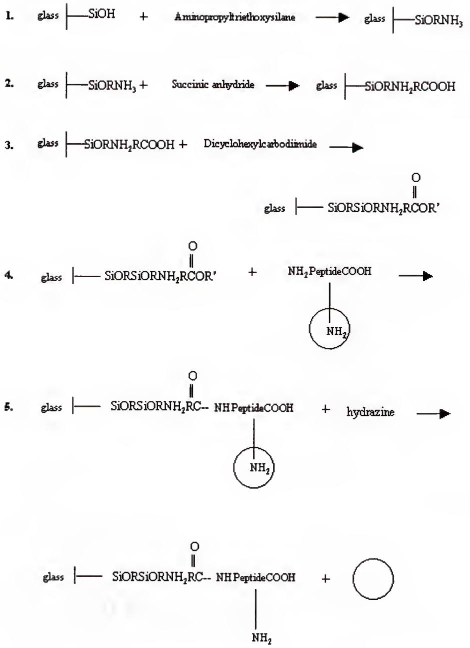

Figure 6-5. Schematic of polypeptide conjugation.

Evaluation of Conjugated Substrates

A batch method was developed to compare the adhesion properties of each surface. While this method could not be used to measure kinetic attachment constants, the experiments were useful in comparing treatments. For this experiment, the attachment of wild type bacteria to surfaces was compared with clumping factor deficient strains, in which cells was suspended in close contact with surfaces adsorbed with or without fibrinogen. For an ideal system, we would expect significant attachment to occur only for the system consisting of clumping factor positive bacteria and adsorbed fibrinogen fragments (Fig 6-6).

Expected Attachment Rate for Ideal Substrates

	Ligands Present	No Ligands Present
Wild Type Strains	HIGH	LOW
Clumping Factor Negative Strains	LOW	LOW

Figure 6-6. Expected Attachment rate for Ideal Systems

As a test, bare slides as well as slides conjugated to control and active peptides were incubated in bacteria suspensions of 45 E6 cells / ml for one hour. The slides were then washed lightly, and placed on the microscope for counting. For each slide, ten measurements of cell density were recorded and the average and uncertainty of results are shown in Figure 6-7. While S. *aureus* was able to attach to cross-linked slides, the attachment to bare glass was also significant, meaning that non-specific interactions promoting adhesion were taking place.

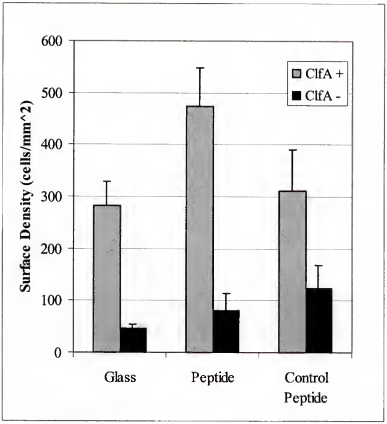

Figure 6-7. Evaluation of modified microscope slides via batch experiments. Adhesion of bare glass slides compared to active peptides and control peptides (inactive).

As seen in the figure, glass conjugated with the 12 residue polypeptide was only slightly more effective in binding wild type *S. aureus* cells than plain glass. Furthermore, a significant number of wild type strains adhered to the control peptide isomer, meaning that non-specific effects were also significant. Because these effects limit the extent to which specific adhesion may be characterized, a system needed to be developed where only specific adhesion is observed and non-specific adhesion is minimized.

Selection and Evaluation of Adsorbed Proteins

Because bioconjugated slides were unable to control for non-specific interactions, whole fibrinogen and combinations of other non-specific blocking agents were instead adsorbed directly to the microscope slide surface and the corresponding interactions with bacteria suspensions were measured. The many combinations of fibrinogen and blocking proteins were tested using a parallel plate flow cell technique. Because the flow cell design allows for individual microscope slides to be treated and assembled to the chamber prior to use, the preparation method used in the measurement of surface forces also suitable for use for use in flow experiments. Both the technique and method of analysis has been previously developed (Rut98). Since slight modifications were made including the use of both a syringe pump and smaller flow chamber, the pertinent experimental details are described below.

Parallel Plate Flow Cell Apparatus and Measurement

The parallel plate flow cell, purchased from CytoDyne Corporation (San Diego, CA) is illustrated in Figure 6-8. It consists of a transparent, polycarbonate plate to which inlet and outlet ports have been bored. Circumscribing the top surface is a rectangular, depressed groove that makes up the vacuum chamber. To assemble the cell, suspension fluid is passed through the inlet port until a large bead of water appears on the surface. A 25×75 mm glass slide is then depressed onto the bead, and is held in place by vacuum pressure. A 200-micron spacer gasket separates the microscope slide from the polycarbonate chamber. Once the chamber is assembled, it is then mounted upside down on an inverted microscope. The image is collected by a frame grabbing board and displayed on an external monitor. The images are then stored and processed using image analysis macros. When the suspension is passed through the PPFC, a real time display reveals the flowing bacteria attaching to the microscope slide surface.

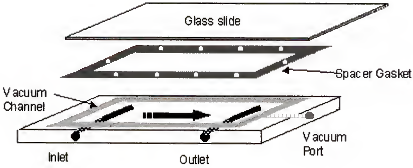

Figure 6-8. Parallel Plate Flow Cell Apparatus

Measurement of the intrinsic rate constant

To determine the intrinsic rate constant, an *effective* attachment rate constant must be measured as a function of downstream position. Therefore measurements of surface concentration $c_s(x, t)$ and a measurement of inlet (i.e., bulk) concentration c_0 are required. The inlet concentration is measured directly using a Petroff-Hausser counting chamber where as surface concentrations are generated by the following method. An OPTIMAS program has been written to recursively scan over the flow cell and collect images as a function of time and position (Rut98). The program sends signals to a motorized stage, where position and time data are recorded. For each of the ten downstream (x) positions, an image is taken at four different y positions, and the stage returns to these same forty positions over the course of the experiment (Figure 6-9). Determination of cell concentration is made using an automated image analysis procedure that counts the number of cells in a given field of view. The user determines the minimum number of adjacent pixels that constitute a bacterium. By selecting discrete upper and lower brightness thresholds corresponding to typical bacteria images, the user is able to count the cells in each frame automatically.

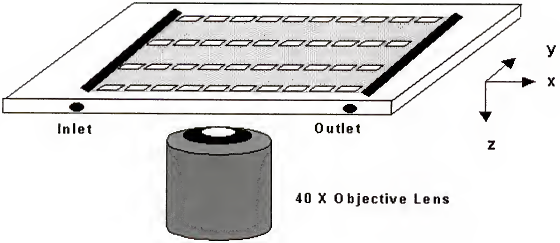

Figure 6-9. Regions of interest on the PPFC

Cell attachment rate constants have been measured using similar flow, automation, and detection schemes, the goal of which is to measure the change in surface concentration as a function of time (Sjo90, Mei94). Assuming a uniform concentration of cells in the medium and applying first order attachment kinetics, the overall attachment rate constant k_{eff} for such a system is determined from equation (6-1).

$$\frac{dc_s}{dt} = k_{eff} c_b ; \tag{6-1}$$

where c_b is the density of cells in the bulk and dc_s/dt is the rate of increase of cell surface density. Each of these parameters represents a measured quantity.

For various shear rates and surface potentials, the assumption of constant concentration throughout the flow cell may not hold. Convection forces as well as diffusion due to Brownian motion affect the overall attachment rate k_{eff}. The accumulation or depletion of cells near the surface (< 1 μm) may lead to cell concentrations that are dependent on both downstream and axial distance. To combat this issue, transport models have been constructed that relate the measured attachment constant and flow parameters to a single intrinsic rate constant (Dic95b). The determination of an intrinsic constant is advantageous because it not only accounts for downstream depletion of cells in the bulk solution, but also is used to predict overall attachment rates in other experimental or *in-vivo* systems.

The application of a boundary layer model accounts for the convective-diffusive flow of particles within the cell, so that the determination of the intrinsic attachment rate k_+ is independent of flow properties and will only on surface interactions. A two dimensional model was developed to determine a single intrinsic attachment rate constant that is independent of flow conditions (Rut98). The description of this model is shown below.

A surface force boundary layer approximation is adopted which defines two fluid regions in the area normal to the flow surface: an interaction region near the surface and a bulk region, where surface forces are insignificant. This distance is set at an arbitrary distance normal to the surface (~one cell diameter) Γ, which defines the distance where an attachment event can take place.

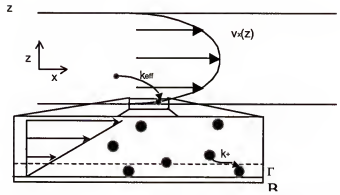

Figure 6-9. Illustration of convective-diffusive transport model for bacterial attachment within a parallel plate flow cell.

The attachment rate of cells to the surface is assumed to be proportional to the concentration of cells at the boundary layer distance, Γ. Steady state dictates that the transport rate of cells into the boundary layer $-J_z$ equals the irreversible attachment rate at the surface. Thus,

$$\frac{dc_s(x,t)}{dt} = -J_z(x,\Gamma) = k_+ c(x,\Gamma) \tag{6-2}$$

Equating (6-1) and (6-2) yields

$$\frac{k_{eff}(x)}{k_+} = \frac{c(x,\Gamma)}{c_0} \tag{6-3}$$

In the bulk region, the flux is dependent only upon diffusion and the effect of gravity, thus:

$$J_z(x,z) = -D\frac{\partial c}{\partial z} - Vc \qquad z \geq \Gamma \tag{6-4}$$

where V is the settling velocity. Assuming negligible surface interaction and diffusion in the x direction relative to convection, the convective diffusion equation in the bulk region at steady state is:

$$0=-v_x(z)\frac{\partial c}{\partial x}+D\frac{\partial^2 c}{\partial z^2}+V\frac{\partial c}{\partial z} \qquad z\geq \Gamma \qquad (6\text{-}5)$$

where $v_x(z)$ is the downstream fluid velocity. This homogenous, 2nd order linear partial differential equation requires one initial condition and two boundary conditions for solution. Assuming that no attachment has occurred at the inlet ($x = 0$), the initial condition is expressed as:

$$c(0,z)=c_0 \qquad (6\text{-}6)$$

Far above the boundary layer, the cell concentration is assumed to be identical to the bulk concentration, thus,

$$c(x,z>>\Gamma)=c_0 \qquad (6\text{-}7)$$

Choosing c_0, chamber length L, and diffusivity / sedimentation velocity D/V, as the relative dimensions, equation (6-5) can be rewritten as:

$$\frac{\partial u}{d\xi}=\frac{1}{\beta(y-\eta y^2)}\left(\frac{\partial^2 u}{\partial y^2}+\frac{\partial u}{\partial y}\right), \qquad (6\text{-}8)$$

where $u = c/c0$, $\xi = x/L$, $\eta = D/(Vh)$, and $\beta=\frac{SL}{V}\left(\frac{D}{LV}\right)^2$. The non-dimensionialized initial and boundary conditions are rewritten as:

$$u(\xi=0,y)=1 \qquad (6\text{-}9)$$

$$u(\xi,y=H)=1 \qquad (6\text{-}10)$$

$$\left.\frac{\partial u}{\partial y}\right|_{y=\Gamma}=(\alpha-1)u(\xi,\gamma) \qquad (6\text{-}11)$$

where $\gamma=\Gamma v_s/D$, and $\alpha=k_+/v$, and $H>>1$ is the chosen upper boundary difference. Equation (6-8) was then solved numerically using a centered finite difference approximation of the y-domain ($\Gamma<y<H$). The model can be solved for given values of

parameters γ, η, α, and β. To extract intrinsic constants from experimental data, γ, η, and β are measured quantities, while α is the fitted parameter used to determine k_+.

Evaluation of Bovine Serum Albumin

Protein adsorption

The objective of the following experiment was to test the effectiveness of bovine serum albumin as a potential blocking agent in *S. aureus* adhesion studies. The bovine serum albumin coated microscope slides were prepared by submerging previously chromerge treated 25×75 mm microscope slides (Fisher) in a in a 0.5 wt% BSA solution (Sigma-Aldrich, St. Louis, MO) in Dulbecco's phosphate buffered saline solution (Life Technologies, Rockville MA) and stirred for two hours. Fibrinogen coated slides were prepared by first submerging identical slides in a stirred 0.02 mg / ml human fibrinogen (Sigma-Aldrich) solution for two hours followed by submersion in the 0.5 wt% BSA solution.

Parallel Plate Flow Cell operation

The intrinsic rate attachment constant of both wild type and clumping factor deficient strains to both bovine serum albumin and human fibrinogen coated surfaces was measured using the parallel plate flow cell technique previously described. The experimental procedure, similar to the previous study (Rut98) was updated slightly and is described below.

Bacteria cultures were grown in tryptic soy broth (Difco, Sparks MA) at 37° C for 16 hours. The culture was centrifuged, decanted, and resuspended in Dulbecco's phosphate buffered saline. This process was then repeated twice to remove all traces of nutrient broth, and the final suspension was sonicated lightly to break up clusters. The suspension was then counted using a Petroff-Hausser counting chamber in conjunction with automated video microscopy and diluted to a final concentration of 20E6 cells/ml. Once the flow lines are connected, and the silicone seal is put into place, plain PBS is pumped through the inlet at a rate of 1 ml / minute.

After selecting the location of the 40 fields of interest, each field was focused on the microscope slide surface, and x, y, and z positions were recorded. After the focal point of each field was stored, the bacteria suspension was sent through the flow cell and an OPTIMAS™ macro collected between 15 and 30 sequential images at approximately two-minute intervals. Upon completion of the experiment, the images were saved and an additional macro was used to count the number of attached bacteria for each field at each time interval. To determine the effective rate attachment constant for each run, a plot of cell density vs. time was generated, and slopes were calculated for each field. The rate attachment constant k_{eff} was calculated according to Equation 6-1 and averaged.

Figure 6-10 illustrates the results of this study. From the graph, we deduce that the wild type strain 54 exhibits a positive adherence to fibrinogen and that bovine serum albumin would make a poor choice as a non-specific blocking agent because the attachment rate to BSA was only 25% less than that of fibrinogen. While the expected clumping factor mediated interactions are stronger, they do not agree with similar studies that found the ratio of specific to non-specific binding to be as high as 10 to 1. It is possible that the clumping factor protein is interacting with the albumin coat, perhaps through trace amounts of fibrinogen molecules remaining in albumin, which has not been further purified. The clumping factor negative strain, A2, was approximately 70% less adherent to BSA. This finding indicated that the BSA either did not completely coat the microscope slide, or that other mechanisms facilitated binding, such as other proteins existing as impurities of BSA.

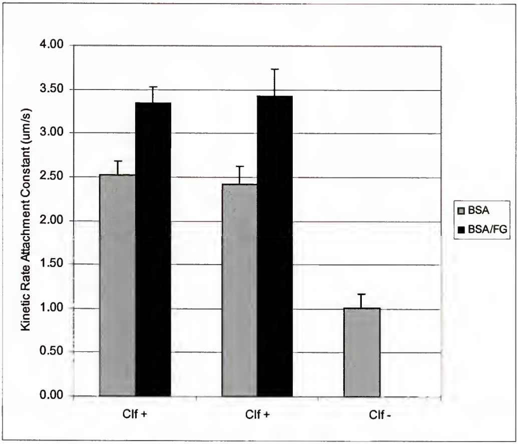

Figure 6-10. Comparison of Attachment to Bovine Serum Albumin and Human Fibrinogen.

Evaluation of Human Serum Albumin, Skim Milk, Casein, and β-Casein

Besides bovine serum albumin, typical proteins used as non-specific "blocking agents" for glass plates include porcine thyroglobin (PTG), high-density lipoprotein (HDL), porcine skin gelatin (GEL), casein (CAS), and bovine milk (Vog87). It is commonly accepted that these high molecular weight proteins adsorb on glass and other solid surfaces to form a thin coating in physiological electrolyte conditions (Bro00a). The properties (i.e., surface charge, surface density) and conformations of these protein films are dependent on factors such as upon the substrate charge and hydrophobicity (Uye90, Kul97).

Ruling out BSA as a possible non-specific blocking agent, experiments were then repeated with the exception that human serum albumin (HSA), skim milk, casein (CAS), and beta-casein (β-CAS) were employed as non-specific agents. Parallel plate flow cell experiments were performed as described previously, with the addition that intrinsic rate attachment constants were calculated using the boundary layer model. Figure 6-11 shows the observed dimensionless intrinsic rate constant k^+ (scaled to settling velocity) for each surface.

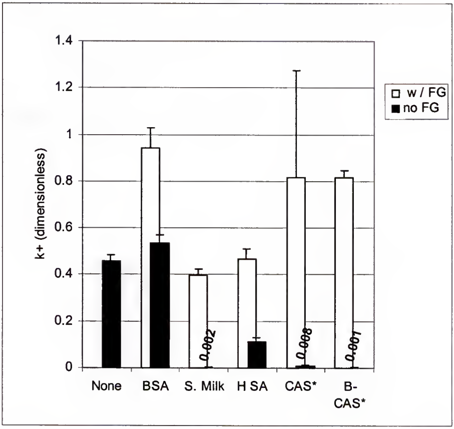

Figure 6-11. Dimensionless rate attachment of *S. aureus* to test substrates

From the chart, it is clear that both bovine serum albumin (BSA) and human serum albumin (HSA) were ineffective in blocking non-specific adhesion. Adhesion was surprisingly greater to bovine serum than for bare glass, indicating the possibility that specific reactions were taking place. As expected, skim milk completely eliminated all non-specific binding, therefore casein, the most prevalent protein in milk, was employed. β-casein was ultimately chosen as the non-specific blocking agent because its ability to form monolayers (Nyl97) and thus will be the protein of choice for use in flow cell experiments as well as 3DOT-EWLS experiments.

CHAPTER 7
MEASUREMENT OF SPECIFIC INTERACTION FORCES

With systems in place for both deposition measurement under well-defined flow conditions and direct force measurement on single, viable cells, a series of experiments was performed to investigate the effect of adhesin length on the bacterial attachment process. Previous experiments using these mutants revealed an increasing dependence of MSCRAMM length on measured attachment rate constants (Rut98). Because substrate preparations made use of skim milk as a non-specific blocking agent, subsequent contamination and scattering of milk solids prohibited successful employment of EWLS-3DOT measurements.

Efforts taken to improve upon substrate preparation have allowed for force measurements between *S. aureus* and proteins where bovine β-casein (a component of milk) was employed as a blocking agent. In an effort to correlate force-measurements with deposition rates using these improved substrates, a series of experiments was designed in conjunction with Jessica Brown that led to a detailed description of intrinsic attachment rate (k_+) as a function of MSCRAMM length (Bro00b). These experiments were performed at several shear rates and as in the case of Ruta 1998, and results indicated that attachment rates had both an increasing and saturating dependence on MSCRAMM stalk length.

Materials and Methods

Measurements of bacterial attachment rates to surfaces were made using the Parallel Plate Flow Cell protocol described in Chapter 6. Substrates were prepared by pre-treating glass microscope slides in Chromerge Cleaning Solution (Fisher) and allowing the slides to dry completely. Solutions of 0.18 mg/mL β-casein (Sigma) and 0.02 mg / mL human fibrinogen (Sigma) were prepared in Dulbecco's Phosphate Buffer Solution and then filtered using by 0.22 micron vacuum or syringe filters (Millipore, Bedford MA). To prepare surfaces displaying active clumping factor binding sites, a droplet of fibrinogen was allowed to incubate on the microscope slide surface for two hours. Following fibrinogen deposition, the microscope slide was quickly immersed in PBS, and a subsequent droplet of β-casein was allowed to incubate on the surface for two additional hours, ensuring for complete coverage of the microscope slide surface.

Kinetic Rate Attachment Measurements of Mutants with Varying Clumping Factor Length

With the mutant strains and parallel plate flow cell methodology described in Chapter 6, Jessica Brown performed several sets of parallel plate flow cell deposition experiments (Bro00b). Abbreviated results from this study are shown in Figure 7-1 where the intrinsic attachment rate of bacterial deposition is plotted for *S. aureus* mutants expressing clumping factor of varying length and activity. Stalk lengths are reported based upon an estimated alpha-helical coil structure. Experiments were performed at a shear rate of 100 s^{-1} and the mean and uncertainty (weighted average values of triplicate runs) are shown in the graph.

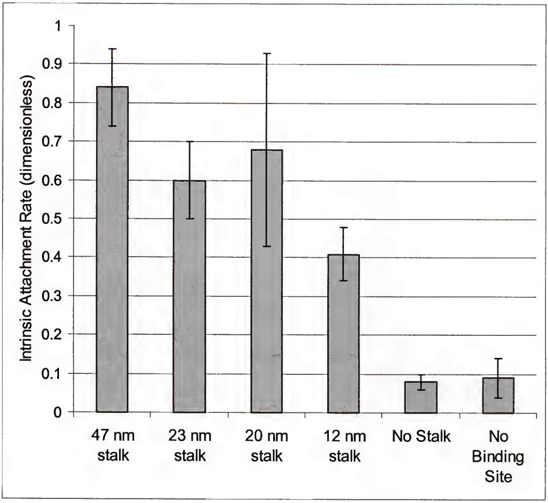

Figure 7-1. Attachment rate of various mutants to adsorbed fibrinogen and B-casein.

While Figure 7-1 does not reveal a monotonically increasing dependence of attachment rate on stalk length, a positive correlation exists that seems to saturate at longer stalk lengths. Mutant strains devoid of either binding site or stalk failed to adhere appreciably to adsorbed fibrinogen under flow, and these results were consistent with previous studies (Har97).

Force Distance Profiles for Mutants with Varying Clumping Factor Length

Using the force measurement procedure described in Chapter 3, equilibrium force distance profiles were performed for a selection of *S. aureus* mutants, where force is plotted as a function of separation distance. Results of the study are shown in Figure 7-2.

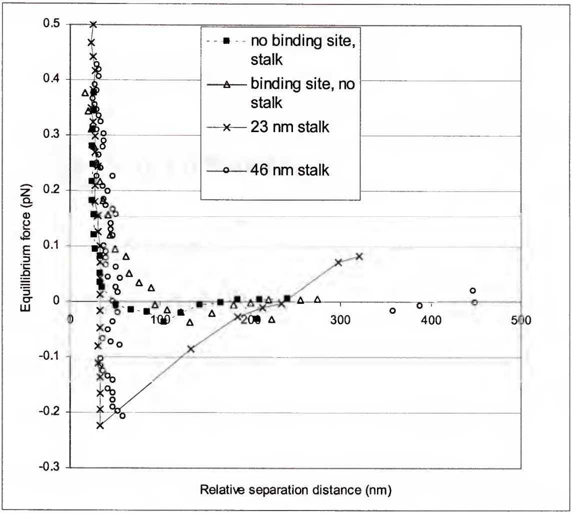

Figure 7-2. Equilibrium force distance profiles for *S. aureus* mutants.

From the plot, it is clear that the mutant strain devoid of a binding site exhibited a force-distance profile that was purely repulsive in nature. In fact this result was very similar to the surface force measurements taken between wild type *S. aureus* and β-casein, where repulsive forces were observed at approximately 80 nm from the microscope slide surface. While only one experimental run is illustrated in the plot, observation of several experimental measurements indicate that at the conclusion of experimental runs, the bacteria remained unattached to the surface upon disengagement of the optical trap. Even at trap focus positions corresponding greater than 0.5 pN of actuated force, the presence of adsorbed protein on the microscope slide prevented the adhesion of bacteria. This result indicated that bacteria devoid of clumping factor mutants were neither able to interact specifically with adsorbed fibrinogen on the slide, or interact with bare glass on the surface.

Equilibrium force measurements between mutant strains expressing clumping factor containing active binding but with no stalk region also produced repulsive interactions. However, at the conclusion of these experiments, visual observations indicated that during the experiments (but outside of the region of linear force assumption), stalk deficient but active site expressing mutants attached to the fibrinogen-coated surface. These events indicated that even though repulsive interactions were measured between cells and surfaces, the optical trapping force provided a sufficiently close contact and long duration to allow for specific binding.

Force measurements between mutants expressing both active binding sites and long, defined stalk regions revealed attractive force measurements. In addition, force-distance profiles illustrate large gaps in cell separation distances indicative of cell attachment during the measurement. Upon trap disengagement at the conclusion of the experimental run, intensity variance measurements (data not shown) combined with visual observation of lateral particle fluctuations indicate that both the 23 nm stalk mutant and the 46 nm stalk mutant interacted irreversibly with the fibrinogen coated surface.

Additional information may be realized by comparing both the distances at which attractive interactions were first observed as well as the attachment span. As seen in Figure 5-2, the 23 nm mutant moved approximately 80 nm from the last diffusing position to a firmly attached state. The 46 nm mutant moved nearly 300 nm from the last diffusing position to the firmly attached state, indicating that attractive forces were able to act on the particle at trap positions significantly larger than the stalk length.

Discussion of Results

The results of the correlated parallel plate flow and EWLS-3DOT experiments are summarized in Table 7-1. Column two shows the kinetic rate constant as measured by parallel plate flow cell and columns three through five show the key results as measured by the 3DOT-EWLS apparatus.

Table 7-1 Summary of Combined PPFC and EWLS-3DOT Apparatus

Mutant Type	**Kinetic Rate Constant**	**Attractive Forces Measured?**	**Did Particle Attach?**	**Attachment Distance**
No Stalk, No Binding Site	0.09 ± 0.05 (dimensionless)	No	No	N / A
No Stalk, Binding Site	0.08 ± 0.02	No	Yes	un-detectable
23 nm Stalk	0.60 ± 0.10	Yes	Yes	80 nm
46 nm Stalk	0.84 ± 0.10	Yes	Yes	300 nm

From the table it is apparent that the presence of both binding stalk and binding stalk has a great effect on the ability of bacteria to attach to adsorbed fibrinogen. However, the fact that cells devoid of binding sites were able to adhere at all to the chamber is an important consideration. Plausible explanations for this adherence could be that an incomplete coverage of protein was formed on the microscope slide surface or that the protein layer was in some way disturbed by the shear rate at the slide suspension interface. Low kinetic attachment rates are also supported by the fact that only repulsive energies were measured using the force measurement procedure and that the optical force applied to the surface over several minutes of experimentation was not sufficient to stimulate an attachment event.

Mutant strains expressing a binding site on the surface without the spacer stalk also adhered poorly to fibrinogen under flow. When probed against the surface, only repulsive forces could be measured. However, during data collection, when the bacterium was held in close proximity to the fibrinogen surface for several minutes, an irreversible attachment was observed, indicating that a specific binding event took place. Poor attachment within the parallel plate flow cell indicates that either the time required is insufficient or that the distance between the clumping factor adhesins and fibrinogen binding sites is too great for an attachment to take place under flow conditions.

Enhanced attachment of mutants expressing spacer stalks under flow conditions is supported by the observation of attractive forces as well as defined attachment events during force measurement. The fact the jumps to the surface for the 23 nm mutant and 46 nm mutant are in excess of 80 nm and 300 nm respectively is troublesome especially considering that only shorter-range cell-surface would be predicted at such a high electrolyte concentration. However, if one considers the trap position and corresponding distribution of cell positions prior to attachment, the point plotted on the abscissa only represents the mean of positions. Instantaneous measurements show that the diffusing cell can occupy a distance in excess of 60 nm due to Brownian motion. Combined with the fact that the surface structure of the adsorbed fibrinogen may be loosely structured, a single binding event initiating a cascade of subsequent bond formations is the proposed mechanism leading to attached enhancement. This hypothesis of extremely fast binding is supported by models predicting that such bond formations at large separation distances are far less thermodynamically favorable than can states characterized by many bonds and short distances.

The measurement techniques employed in this study do not offer conclusive evidence to place the actual location of the stalk with the respect to the cell wall and membrane. However results of this combined study seem to indicate the presence of the stalk is required for enhanced deposition under flow and is not required for specific binding to occur. This suggests that when binding sites are displayed in the absence of a stalk, these sites may not extend at a distance at which enhanced deposition may take place. Because of its hydrophilic serine--aspartate repeating units, the stalk region is expected to form a stable structure in physiological conditions. Therefore it would appear that the stalk serves the physiological function of enhancing adhesion by reducing the distance between clumping factor binding site and fibrinogen ligand.

CHAPTER 8
CONCLUSIONS AND SUGGESTIONS FOR FUTURE WORK

Conclusions

Improved understanding of the bacterial adhesion process can ultimately result in useful applications, such as the design of infection-resistant biomaterials or the development of high-specificity filters capable of removing specific organisms based upon their distinct surface properties. In this work, novel methodologies have been employed to improve the understanding of the physicochemical mechanisms of bacterial adhesion to solid surfaces. While the number and complexity of cellular adhesion models is both widespread and sometimes controversial, the tools available to evaluate these models are few. By adapting a recent colloidal force measurement technique (Cla01) for use with bacteria, a method for evaluating and comparing bacterial interaction models was developed.

To demonstrate the effectiveness of the technique, interaction forces between bacteria and bare glass were measured and compared to DLVO theory at low electrolyte concentrations. *Staphylococcus aureus*, because of its near-spherical shape and well-defined surface structure, was chosen as model organism. Equilibrium force results agreed quite well with DLVO theory for electrolyte concentrations below 1.5 mM KCl, and deviated slightly at larger electrolyte concentrations. Applications of this technique were then extended to allow for surface measurements in high electrolytes and physiological conditions, so that the forces between single bacteria and protein-coated surfaces could be measured. When *S. aureus* was probed against bare glass in high electrolyte conditions, attractive interactions were observed, and the trajectory of the particle moving toward the surface was analyzed. However, when strains of *S. aureus* were probed against β-casein, repulsive forces were measured, indicating that steric interaction forces served to impede attachment of bacteria in the absence of specific interactions.

Through the development and testing of several schemes capable of demonstrating adhesin-mediated binding, a substrate was developed so that the effect of MSCRAMM length on attachment probability and interaction forces could be tested and interpreted. Mutant strains expressing specific fibrinogen-binding proteins of various lengths and activities were made available by collaborators, which allowed for a significant hypothesis relevant to the pathogenic infection of biomaterials to be further evaluated: that the repeat region within bacterial MSCRAMM's promotes bacterial adhesion based upon its length. Correlated deposition results using parallel plate flow cell methodology in conjunction with EWLS-3DOT measurements described above, revealed that the repeat or "stalk" region within the cell surface protein "clumping factor" allowed *S. aureus* to overcome energy barriers normally present on protein-coated surfaces. This example indicates that physiological interactions such as MSCRAMM binding can be evaluated by EWLS-3DOT because both the distance and time at which cells may interact with the surface can be defined and controlled by the user.

Suggestions for Future Work

Because application of the optical trapping method allows the user to non-invasively manipulate and confine cells in close proximity to user-defined surfaces while measuring separation distance measurement in real time, a range of interaction forces and measurement conditions can be explored that would not be possible using competing methods such as AFM or TIRM. Limitations in applicability exist, however, and examples of improvements to extend the usefulness of the technique are described below. Specific suggestions to improve the elucidation of physico-chemical mechanisms using the clumping factor-fibrinogen system and others are also described.

Improved Optical Trap

A new optical trap has been designed to replace the current system the schematic of which is shown in Figure 7-1.

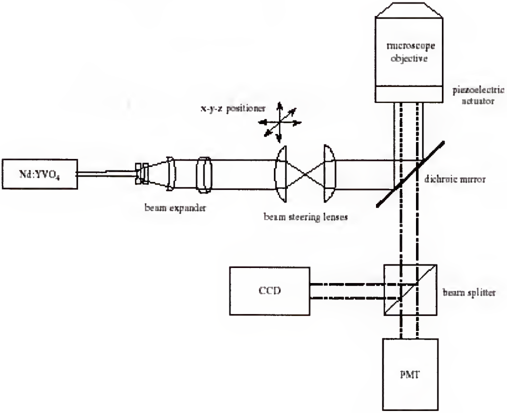

Figure 8-1. Schematic for a custom optical trapping system.

The new trapping system uses a 1.5 W Nd:YVO4 solid state laser (l=1064 nm) with an adjustable power control, high precision optical components to minimize spherical aberration effects, a three-axis mounted aplanatic lens for steering the beam laterally, and a single-axis piezoelectric positioner for repeatable nanometer-scale movements of the trapped particle (Cla01). The new system offers considerable benefits over the commercially available optical trap currently employed in that the user is able to position the particle using motorized lenses as opposed to a stage motor, which suffers from hysteretic effects. Furthermore, lens adjustments and modifications may be made to optimize the symmetry of the trapping gradient so that shape-induced torque effects are minimized.

Improve Measurement of Specific Interactions of Bacteria with Coated Surfaces

One of the difficulties in performing specific interaction measurements was that attractive forces were in excess of the trapping strength over a critical range of separation distances. On approach to the surface, the bacterium spontaneously jumped to the surface from a particular distance. By adjusting the power of the trapping laser described in Figure 8-1, the range of unknown separation distances can be reduced significantly. It is important to realize that when a cell is at the energy minimum and bound to the substrate, attractive forces acting on the cell at that moment are not known absolutely. Rather, the forces can only be shown as greater than the applied optical force acting on the cell at that trap position.

Employment of the piezo-electric stage can be used to further investigate the magnitude of attractive forces by allowing the user to reverse directions of the trap, without suffering the hysteretic effects normally associated with the direction changes when using the stage motor. Such a scheme will allow for force measurements in both forward and reverse directions and will be able to map interaction forces in a more comprehensive way.

While the results presented in this dissertation represent the first time optical forces have been use to non-invasively measure the specific interactions of whole bacterial cells with biological substrates, insufficient information is known about the measurement system to make straightforward comparisons with existing models, as has been done for the case of DLVO forces. To make comparisons with specific attachment models, the surface characterizations of the specific binding models involved must be better defined. Such models generally require that the surface density and orientation (unstretched bond length) of the molecules involved be defined (Dic97). While the surface density of clumping factor protein has been estimated by radio-labeling, the use of adsorbed fibrinogen as means for displaying binding site may not provide an accurate means of controlling bond position, as the molecule large relative to the interactions involved, and that multiple layers of fibrinogen may be present. It is recommended that the smallest fibrinogen fragment able to mediate specific binding be immobilized to a surface in such away that both specific interaction is pronounced and that active site density is controlled.

Even if both the surface densities and reaction propensities are explicitly known, the current methodology is only able to recognize attachment events and cannot identify MSCRAMM binding as it occurs, therefore force or energy profile will have to be mapped using a stochastic analysis that measures the probability of attachment for a given set of conditions.

Ideally, a measurement system used to measure specific interaction forces should allow for simultaneous indication of particle positions and bond formations. This system would have to consider an interaction energy surface that accounts for both non-specific forces (along the separation distance axis) and specific binding forces (along an axis indicative of the number of bonds). While such a system is not currently envisioned for proteins expressed on living surfaces, model systems consisting of microbeads and surfaces each containing bioconjugated receptor-ligand molecules on their surfaces have been proposed. By modifying bioconjugate pairs with molecules able to indicate bond formation (such as the use of fluorescence resonant energy transfer), further mechanisms of the bacterial adhesion process may be elucidated

APPENDIX

FORCE MEASUREMENT DATA ANALYSIS PROGRAM

This appendix contains the image analysis program used in the calculation of force-distance profiles. For each experimental run, intensity data is stored as a function of relative trap position and stored as a MS-Excel Data File. Once this information is loaded into MATLAB, the following program (m-File) is used to read the data file, perform the optical trap calibration, determine absolute separation distances, and calculate the equilibrium and viscous forces.

It should be noted that Richard Dickinson performed the majority of the code writing contained in the program and Aaron Clapp also made many necessary corrections and updates. While Richard Dickinson is considered to be the primary author of this program, it is included in the appendix for completeness and for the fact several additional corrections and comments were required for the technique's application to bacterial systems.

```
% analyze.m

%

% A data analysis program for calculating static and dynamic interactions
% of a trapped colloidal particle near a flat plate

% (last revised 12/18/2001)

% required function files      gInfunc.m theoretical intensity autocorrelation function
%                               gImin.m fits autocorrelation function
%                               gImin2.m fits autocorrelation function using additional
%                                     weight for shot noise
%                               brenner.m calculates correction to Stokes law (from
%                                   Brenner's theoretical result)
%                               dispn.m
%                               findmode.m  calculates mode of distribution
%                               dfunc.m function that fits drag coefficient data to find %
                                    absolute positions
%                               auto.m calculates autocorrelation function

%
% NOTES:
%
%  variables that begin with "n" indicate a NUMBER or length of a vector (single value),
as in "ndata"
%  variables that begin with "m" indicate a MATRIX of numbers, as in "mback"
%  data set must be named "fulldata" for program to work properly
%  units are shown in brackets

hold off;

% COMMONLY ADJUSTED EXPERIMENTAL PARAMETERS (ADJUST FOR
%  EACH NEW DATA SET)

ndata=65536;            % total number of samples acquired at each trap position
freq=40000;             % sampling frequency [Hz]
pendepth=135;           % evanescent wave penetration depth [nm]
R0=500;                 % estimated particle radius [nm]
tau=150e-6;             % time constant of low-pass filter [s]

%% USER-DEFINED DATA RANGES (ADJUST FOR EACH NEW DATA SET)

mback=1:15;          % data point range used to estimate background mean and variance
mstiff=30:50;        % data point range used to estimate the trap stiffness
mdrag=50:70;         % data point range used to estimate absolute separation distance
nskip=10;            % number of data points to skip at the end of the data set

%% PARAMETERS AND CALCUATED VALUES THAT ARE TYPICALLY FIXED

mcal=min(min(mdrag),min(mstiff)):max(max(mdrag),max(mstiff));
% data point range for all calibration

ncal=length(mcal);        % number of points in entire calibration range
nstiff=length(mstiff);    % number of points in stiffness calibration range
sigR=.01;                 % fractional uncertainty in the particle radius "R0"
eta=0.00085;              % viscosity of fluid [kg/m· s]
nfluid=1.333;             % refractive index of fluid (water at 25°C)
nglass=1.515;             % refractive index of glass plate (BK-7 glass)
```

```
refratio=nfluid/nglass;    % scaling factor for separation distances (refractive index ratio)
kT=1.38e-23*298;           % thermal energy at 25°C [J]
ndata=ndata+1;             % add one to account for trap position in data header
ntrap=round(length(fulldata)/ndata)-1;
                           % calculated number of trap positions based on data set length
beta=1/pendepth;           % inverse penetration depth [nm^-1]
dt=1/freq;                 % sampling time interval [s]
nauto=100;                 % number of data points used in the autocorrelation function fit
tg=dt*(0:nauto-1);         % defines time sequence for autocorrelation function [s]
nsave=ntrap-nskip;
              % defines the length of the data to be analyzed (ignores skipped region)
mplot=mcal(1):nsave;
% data point range to plot beginning with first point of calibration region

options=optimset('Display','off','TolX',1e-4);
% set options for 'fminsearch' algorithm


%% INITIALIZATION OF VARIABLES AND MATRICES

ztrap=zeros(1,ntrap);              % vector containing the trap positions
meanI=zeros(1,ntrap);              % mean intensity
varI=zeros(1,ntrap);               % variance of intensity


%% PLOT OF UNCORRECTED MEAN AND VARIANCE FOR SELECTION OF
APPROPRIATE CALIBRATION RANGES

for i=1:ntrap
% creates a loop over all trap positions

data=fulldata(((i-1)*ndata+2):i*ndata);
% loads time-series information into temp variable "data"

meanI(i)=mean(data);           % evaluates and records mean intensity
   varI(i)=var(data);          % evaluates and records variance of intensity
   ztrap(i)=fulldata((i-1)*ndata+1);
                               % records all trap positions
end

ztrap=(3000-ztrap)*refratio;

% reverses direction of trap positions and rescales step size to account for refraction

mIcal=meanI(mcal);   % defines mean data over entire calibration range
vIcal=varI(mcal);    % defines variance data over entire calibration range
```

```
zcal=ztrap(mcal);        % defines trap positions over entire calibration range

% plot to ensure fit is in correct part of curve

SUBPLOT(2,1,1)          % plots data on topmost plot of a two plot figure
plot(ztrap,meanI,'yo',zcal,mIcal,'ro',ztrap(nsave:ntrap),meanI(nsave:ntrap),'go',ztrap(mbac
k),meanI(mback),'bo',ztrap(mstiff),meanI(mstiff),'ko');

xlabel('separation distance (nm)');                          % x-axis text label
ylabel('mean intensity (V)');                                % y-axis text label
title('red=drag; black=stiffness; blue=background; green=skipped');
hold off;     % allows future "plot" commands to erase existing graph

SUBPLOT(2,1,2)      % plots data on bottommost plot of a two plot figure
plot(ztrap,varI,'yo',zcal,vIcal,'ro',ztrap(nsave:ntrap),varI(nsave:ntrap),'go',ztrap(mback),va
rI(mback),'bo',ztrap(mstiff),varI(mstiff),'ko');
xlabel('separation distance (nm)');
ylabel('intensity variance (V^2)');
pause;                  % pauses program until user hits any key
hold off;

%% CALIBRATION OF STIFFNESS AND ABSOLUTE SEPARATION DISTANCE

meanback=mean(meanI(mback));   % estimates background mean
varback=mean(varI(mback));     % estimates background variance

% recalculate mean and variance to account for background levels

mIcal=mIcal-meanback;          % subtract background mean
bvz=zeros(1,ncal);              % initialize vectors
tc=zeros(1,ncal);
etc=zeros(1,ncal);
ebvz=zeros(1,ncal);
edels=zeros(1,ncal);
dels=zeros(1,ncal);
s2=zeros(1,ncal);

j=0;                            % initialize index value "j"

for i=mcal
% loop over all trap positions used for absolute distance calibration

   tg=dt*(0:nauto-1);          % calculate time sequence for autocorrelation function [s]
   j=j+1;                      % create new index "j" that begins with j=1
   data=fulldata(((i-1)*ndata+2):i*ndata)-meanback;
% load time-series data into temp variable "data" with background subtracted
```

```
   [gI ns]=auto(data,nauto);   % calculate autocorrelation function
   gIn=gI/mIcal(j)^2;           % scaled gI(t)
   parI0(1)=(log(gIn(min(find(tg>3*tau)))+1));
 % initial guess of variance due to particle fluctuations
   parI0(2)=.01;                 % initial guess of relaxation time of particle fluctuations
   parI0(3)=gIn(1)-gIn(min(find(tg>3*tau)));
% initial guess of noise variance assuming noise curve relaxes around 3*tau
   parI=fminsearch('gImin',parI0,options,gIn,ns,tg,tau);
% fit autocorrelation data to model fuction "gImin"; return three parameters
   DI=dispn(parI,ns,tg,gIn,tau);
   bvz(j)=parI(1);
   tc(j)=parI(2);
   s2(j)=parI(3);

   dels(j)=tc(j)/bvz(j);                        % scaled drag coefficient:
dels=delta/kT/beta^2
   tct=tc(j);

   ddels=[dels(j)./[tc(j) -bvz(j)] 0];          % calculate standard errors
   edels(j)=sqrt(ddels*DI*ddels');
   etc(j)=sqrt(DI(2,2));
   ebvz(j)=sqrt(DI(1,1));

   fit=gInfunc(parI,tg,tau);
% calculate autocorrelation function using fitted parameters
   subplot(1,1,1)
   plot(tg,gIn,'ro',tg,fit);                     % plot autocorrelation function fit
   xlabel('time (s)');
   ylabel('G_I(t)/\mu^2');
   title('autocorrelation function');
   axis([0 max(tg) -.2*max(gIn) max(gIn)]);
% set plot axis based on autocorrelation function max values
   pause(1);                                     % pause for 1 second
end


%% ESTIMATE BACKGROUND NOISE VARIANCE OVER STIFFNESS
CALIBRATION RANGE

yy=s2(1:nstiff).*mIcal(1:nstiff).^2;
Sxx=sum(mIcal(1:nstiff).^2)-sum(mIcal(1:nstiff))^2/nstiff;
Sxy=sum(mIcal(1:nstiff).*yy)-sum(mIcal(1:nstiff))*sum(yy)/nstiff;
Syy=sum(yy.^2)-sum(yy)^2/nstiff;
bslope=Sxy/Sxx;
varb=(Syy-bslope*Sxy)/(nstiff-2);
ebslope=sqrt(varb/Sxx);
```

```
bcept=mean(yy)-bslope*mean(mIcal(1:nstiff));
ebcept=sqrt(varb*(1/nstiff+mean(mIcal(1:nstiff))^2/Sxx));
plot(mIcal(1:nstiff),yy,'ro',mIcal(1:nstiff),bcept+bslope*mIcal(1:nstiff));
pause;


%% PLOT STANDARD DEVIATION OF PARTICLE POSITION

psigz=sqrt(bvz(1:nstiff)/beta^2);
epsigz=psigz(1:nstiff)/2.*ebvz(1:nstiff)./bvz(1:nstiff);
wt=1./ebvz(1:nstiff).^2;
wt=wt/sum(wt);
mbvz=sum(wt.*bvz(1:nstiff));
embvz=sqrt(sum(wt.^2.*(bvz(1:nstiff)-mbvz).^2));
sigz=sqrt(mbvz)/beta;
errorbar(zcal(1:nstiff),psigz,epsigz,epsigz,'ko');
axis([min(zcal(1:nstiff)) max(zcal(1:nstiff)) 0 75]);
hold on;
plot([min(zcal(1:nstiff)) max(zcal(1:nstiff))],sqrt([mbvz
mbvz]/beta^2),[min(zcal(1:nstiff)) max(zcal(1:nstiff))],sqrt([mbvz+embvz
mbvz+embvz]/beta^2),[min(zcal(1:nstiff)) max(zcal(1:nstiff))],sqrt([mbvz-embvz mbvz-
embvz]/beta^2));
drawnow;
hold off;
xlabel('trap position (nm)');
ylabel('standard deviation (nm)');
title('standard deviation of position');
pause;


%% ESTIMATE TRAP CENTER POSITION

bz=beta*zcal(1:nstiff);
bzrefdat=bz+log(mIcal(1:nstiff))-mbvz/2;
bzref=sum(wt.*bzrefdat);
zj=ztrap-bzref/beta;
zcal=zcal-bzref/beta;

zoff=0;

clear meanI varI mIcal vIcal


%% FORCE CALCULATION

zp=zeros(1,length(mplot));
```

```
f=zp;
tct=100*dt;
edels=0*(mplot);
dels=edels;
s2=edels;
mu=s2;
j=0;

for i=mplot                                        % calculates modes at each trap
position
  tg=dt*(0:nauto-1);                                    % define time sequence
  j=j+1;
  data=(fulldata(((i-1)*ndata+2):i*ndata)-meanback);
% load time-series data into temp variable "data" with background subtracted

  mu(j)=mean(data);                                % calculate mean of data set
  s2est=(bcept+bslope*mu(j))/mu(j)^2;              % estimate noise variance
  ds2est=sqrt(varb)/mu(j)^2;
  [gI ns]=auto(data,nauto);
% calculate autocorrelation function "gI" and weights "ns"
  gI=gI/mu(j)^2;                                   % scaled gI(t) by mean squared
  parI0(1)=(log(gI(min(find(tg>3*tau)))+1));       % initial guesses
  parI0(2)=.01;
  parI0(3)=s2est;
  parI=fminsearch('gImin2',parI0,options,gI,ns,tg,tau,s2est,ds2est);
% fit experimental autocorrelation function to theoretical model
  DI=dispn(parI,ns,tg,gI,tau);
  bvzt=parI(1);
  tct=parI(2);
  sign2=parI(3);
  s2(j)=sign2;
  dels(j)=parI(2)/parI(1);                    % measured drag:  dels=delta/kT/beta^2

  ddels=[dels(j)/parI(2) -dels(j)/parI(1) 0];
  edels(j)=sqrt(ddels*DI*ddels');

  errorrat=edels(j)/dels(j);                  % calculate error
  errorbvz=sqrt(DI(1,1))/bvzt;
  errortc=sqrt(DI(2,2))/tct;
  errors2=sqrt(DI(3,3))/sign2;

  fit=gInfunc(parI,tg,tau);
% calculate fitted function for noise portion of curve
  fit2=exp(bvzt*exp(-tg'/tct))-1 ;
% calculate fitted function for particle fluctuations
  subplot(2,1,1)
```

```
   plot(tg,gI,'ro',tg,fit,tg,fit2);          % plot autocorrelation function with fitted result
   xlabel('time (s)');
   ylabel('G_I(t)/\mu^2');
   title('autocorrelation function');
   axis([0 max(tg) -.2*max(gI) max(gI)]);
   pause(1);

   data=nonzeros((data>0).*data);
% force "data" to include only positive valued elements

   data=-log(data)/beta+zoff;                 % change "data" into separation distances

   zp(i)=findmode(data,.3);                    % most probable position "zp"

   f(i)=(zp(i)-zj(i)-zoff)/sigz^2;             % calculates force [kT/nm]
   force=f(i)*1e9*kT;                          % calculates force [N]

   hold off;
   [NN XX]=hist(data,40);                       % calculate histogram with 40 bins
   subplot(2,1,2)
   bar(XX,NN);                                 % plot histogram as a bar graph
   hold on;
   plot(zp(i),0,'ro');                         % plot a single red circle at location of mode
   axis([0 800 0 max(NN)]);                    % change axis to adjust for height of
histogram
   drawnow;
   hold off;
end


%% FIND ABSOLUTE SEPARATION DISTANCE

zfit=zp(mplot)/R0;                                   % scale x-axis data to initial particle
radius estimate
dfit=dels*kT*beta^2*1e18;                            % rescale drag coefficient data to
yield SI units
edfit=edels*kT*beta^2*1e18;
pfit0(1)=500/R0;                                     % initial guesses for fitted
parameters
pfit0(2)=1;
pfit=fminsearch('dfunc',pfit0,options,dfit,edfit,zfit,sigR,R0,eta);
% fit data to model function "dfunc"
zoff=pfit(1)*R0;
% calculate offset distance from fitted parameter "pfit(1)"

I0=exp(-beta*zoff);                        % calculate effective measured intensity at contact
```

```
zp=zp+zoff;

%% PLOT STATIC FORCE RESULTS

SUBPLOT(2,1,1)
plot(zp(mplot),f(mplot)*kT*1e9,'ro');                        % plot static force results
axis([0 max(zp) -.2*max(f*kT*1e9) 1.2*max(f*kT*1e9)]);
dfit=dels*kT*beta^2*1e18;                                    % calculate drag
edfit=edels*kT*beta^2*1e18;                                  % calculate error in drag
xlabel('separation distance (nm)');
ylabel('force (N)');


%% PLOT DYNAMIC FORCE RESULTS

zf=10:round(max(zp));
% generate x-axis vector of separation distances
dtheor=6*pi*eta*pfit(2)*R0*brenner(zf/R0/pfit(2))*1e-9;
 % calculate theoretical drag
SUBPLOT(2,1,2)
plot(zp(mplot),dfit,'ro',zf,dtheor);
% plot drag results and theoretical curve together
axis([0 max(zp) 0 1.5e-7]);
xlabel('separation distance (nm)');
ylabel('drag coefficient (kg/s)');
```

REFERENCES

Achouak, W. (1994) "Physico-chemical surface properties of rhizobacteria and their adhesion to rice roots." *Colloids Surf. B* 3(3):131-137.

Andrade, J. (1985) "Principles of protein adsorption." *Surface and Interfacial Aspects of Biomedical Polymers*. 2: 1-80. Plenum, New York, NY.

Ardehali, R. and Mohammad, S. F. (1993) "Indium labeling of microorganisms to facilitate the investigation of bacterial adhesion." *J. Biomed. Mater. Res.* 27(2): 269-75.

Bakker, D. P., Busscher, H. J., van der Mei, H. C. (2002) "Bacterial deposition in a parallel plate and a stagnation point flow chamber: microbial adhesion mechanisms depend on the mass transport conditions." *Microbiology*. 148 (2), 597-603.

Barabino, G.A., Liu, X.D., Ewenstein, B.M., and Kaul, D.K. (1999) "Anionic polysaccharides inhibit adhesion of sickle erythrocytes to the vascular endothelium and result in improved hemodynamic behavior." *Blood* 93(4): 1422-1429.

Bell, G. I., M. Dembo, Bongrand, P. (1984) "Cell adhesion. Competition between nonspecific repulsion and specific bonding." *Biophys. J.* 45(6): 1051-64.

Boyce, J. M. (1993) "Spread of Methicillin-Resistant *Staphylococcus aureus* in Hospital After Exposure to a Health Care Worker with Chronic Sinusitis." *Clin. Infec. Dis.* 17:496-504.

Brenner, H. (1961) "The slow motion of a sphere through a viscous fluid towards a plane surface." *Chem. Eng. Sci.* 16: 242-251.

Bronzino, J.D. (2000) *The Biomedical Engineering Handbook*. Second Edition Volume II. 1597-1608. CRC Press: Boca Raton, FL.

Brown, J. (2000) "Study of the specific adhesion of *Staphylococcus aureus* to protein-coated surfaces." M.S. Thesis, University of Florida, Gainesville, FL.

Butt, H.-J., Jaschke, M., and Ducker, W. (1995) "Measuring surface forces in aqueous electrolyte solution with the atomic force microscope." *Bioelectrochem. & Bioenerg.* 38: 191-201.

Clapp, A. R., and Dickinson, R. B. (2001) "Direct measurement of static and dynamic forces between a colloidal particle and a surface using a single-beam gradient optical trap and evanescent wave light scattering." *Langmuir*, 17: 2182-2191.

Clapp, A. R., Ruta, A. G., Dickinson, R. B. (1999) "Three dimensional optical trapping and evanescent wave light scattering for direct measurement of long range forces between a colloidal particle and a surface." *Rev. Sci. Instrum.* 70(6): 2627-2636.

Chew, H., Wang, D.-S., and Kerker, M. (1979) "Elastic Scattering of Evanescent Electromagnetic Waves." *Appl. Opt.* 18, 2679-2687.

Chesla, S. E., Selvaraj, P., and Zhu, C. (1998) "Measuring Two-Dimensional Receptor-Ligand Binding Kinetics by Micropipette." *Biophys. J.* 75: 1553-1572.

Costerton J. W., Stewart P. S., Greenberg E.P. (1999) "Bacterial biofilms: a common cause of persistent infections." *Science* 284: 1318-22.

Dankert, J., Hogt A. H., and Feijen, J. (1986) "Biomedical polymers: bacterial adhesion, colonization, and infection." *CRC Crit. Rev. Biocompat.* 2: 219-301.

Darouiche R.O, Raad I.I., Heard S.O., Thornby J.I., Wenker O.C., Gabrielli A. (1999) "A comparison of two antimicrobial-impregnated central venous catheters." *N. Engl. J. Med.* 340: 1-8.

Dee, K.C., Andersen, T. T. , Bizios, R. (1995) "Enhanced endothelialization of substrates modified with immobilized bioactive peptides." *Tissue Engineering* 1:135-145.

Dickinson, R. B. (1997) "A dynamic model for attachment of a Brownian particle mediated by discrete macromolecular bonds." *J. Colloid Interf. Sci.* 190: 142-151.

Dickinson, R. B. (2002) "Surface Behavior of Bacteria." In *Encyclopedia of Surface and Colloid Science*, Marcel Dekker, Inc., New York.

Dickinson, R. B., Cooper, S. L. (1995) "Analysis of shear-dependent bacterial adhesion kinetics to biomaterial surfaces." *AI.Ch.EJ.* 41: 2160-2173.

Dickinson, R. B., Nagel, J. A., McDevitt D., Foster T. J., Proctor R. A., and Cooper, S. L. (1995) "Quantitative comparison of clumping factor- and coagulase-mediated Staphylococcus aureus adhesion to surface-bound fibrinogen under flow." *Infect. Immun.* 63(8): 3143-50.

Doolittle (1984) "Fibrinogen and Fibrin." *Ann. Rev. Biochem.* 53: 195-229.

Dougherty, S. H. (1988) "Pathobiology of infection in prosthetic devices." *Rev. Infect. Dis.* 10: 1102-1117.

Ducker, W. A., Senden, T. J., and Pashley, R. M. (1991) "Direct measurement of colloidal forces using an atomic force microscope." *Nature* 353: 239-241.

Eimlech, J. G., Jia, X., Williams, R. A. (1995) *Particle Deposition and Aggregation: Measurement, Modeling and Simulation.* Butterworth-Heinemann, Oxford.

Engel, A., Muller, D. J. (2000) "Observing single biomolecules at work with the atomic force microscope." *Nat. Struct. Biol.* 7: 715-718.

Ericsson, M., Hanstorp, D, Hagberg, P, Enger, J., and Nyström, T., J. (2000) "Sorting Out Bacterial Viability with Optical Tweezers." *Bacteriol.* 182: 5551-5555.

Frangos, J. A., Huang, T. Y., Clark C. B. (1996) "Steady shear and step changes in shear stimulate endothelium via independent mechanisms--superposition of transient and sustained nitric oxide production." *Biochem. Biophys. Res. Commun.* 224(3): 660-665.

Friese, M. E. J., Rubenstein-Dunlop, H., Heckenberg, N. R., and Dearden, E. W. (1996) "Determination of the force constant of a single-beam gradient trap by measurement of backscattered light." *Appl. Opt.* 35: 7112-7116.

Gardiner, C. W. (1983) *Handbook of Stochastic Methods.* Springer, Berlin.

Gristina A. G., Giridhar G., Gabriel B. L., Naylor P. T., Myrvik Q. N. (1993) "Cell biology and molecular mechanisms in artificial device infections." *Int. J. Artific. Organs* 11: 755-763.

Harden, V.P., Harris, J.O. (1953) "The isolectric point of bacterial cells." *J. Bacterial.* 65: 198-202.

Hartford, O., Francois P., Vaudaux P., Foster T. J. (1997) "The dipeptide repeat region of the fibrinogen-binding protein (clumping factor) is required for functional expression of the fibrinogen-binding domain on the Staphylococcus aureus cell surface." *Mol. Microbiol.* 25(6): 1065-1076.

Hawiger, J., Timmons, S., Strong, D. D., Cotrell, B. A., Riley, M., and Doolittle, R. F. (1982) "Identification of a Region of Human Fibrinogen Interacting with Staphylococcal Clumping Factor." *Biochemistry* 21: 1407-1413.

Hermann M., Jaconi M. E., Dahlgren C., Waldvoge F., Lew P. D. (1990) Neutrophil bactericidal activity against staphylococcus aureus adherent of biological surfaces. *J. Clin. Invest.* 86:942-951.

Hermansson, M. (1999) "The DLVO theory in microbial adhesion." *Colloids Surf., B* 14: 105-119.

Isberg, R. R., Barnes, P. (2002) "Dancing with the host: flow-dependent bacterial adhesion.(minireview)" *Cell*: 110(1): 1-4.

Israelachvili, J.N. (2001) "Intermolecular forces in biology." *Q. Rev. Biophys.* 34(2): 105-267.

Israelachvili, J. N., and Adams, G. E. (1976) "Direct measurements of long-range forces between two mica surfaces in 10-4 to 1 M KNO3 solutions." *Nature* 262: 774-776.

Jucker, B. A., Zehnder, A. J. B., Harms, H. (1998) "Quantification of polymer interactions in bacterial adhesion." *Environ. Sci. Technol.* 32: 2909-2915.

Kristinsson, K. G. (1989) "Adherence of Staphylococci to intravascular catheters." *J. Med. Microbiol.* 28: 249-257.

Kull ,T., Nylander, T., Tiberg, F. (1997) "Effect of Surface Properties and Added Electrolyte on the Structure of β-Casein Layers Adsorbed at the Solid/Aqueous Interface." *Langmuir* 13: 5141-5147.

Lauffenburger, D. A. (1993). *Receptors*., Oxford University Press, New York.

Lee, I. S., Marchant R. E. (2001) "Force Measurements on the molecular interactions between ligand (RGD) and human platelet $\alpha_{IIb}\beta_3$ receptor system." *Surf. Sci.* 491: 433-443.

Liang, O.D., Flock, J.I., and Wadstrom, T. (1995) "Isolation and characterization of a vitronectin-binding surface protein from Staphylococcus aureus." *Biochim. Biophys. Acta.* 1250: 110-116.

Madigan, M. T., Martinko, J. M., Parker, J. (1997) *Biology of Microorganisms*. Prentice, Upper Saddle River, NJ.

Magnusson, K.-E., Dahlgren, C., Maluszynska, G., Kihlstrom, E., Skogh, T., Stendahl, O., Suderlund, G., Uhman, L., and Walan, J. (1983) "Non-specific and specific recognition mechanisms of bacterial and mammalian cell membranes." *J. Dispersion Sci. Technol.* 6(1): 69-89.

Marshall, K. C., Stout, R., Mitchell, R. (1971) "Mechanisms of the initial events in the sorption of marine bacteria to surfaces." *J. Gen. Microbiol.* 68: 337-348.

McDevitt, D., Francois, P., Vaudaux, P., Foster, T.J., (1994) "Molecular characterization of the clumping factor (fibrinogen receptor) of Staphylococcus aureus." *Molec. Microbiol.* 11(2): 237-248.

McDevitt, D., Francois P. , Vaudaux P., Foster T. J. (1995) "Identification of the ligand-binding domain of the surface-located fibrinogen receptor (clumping factor) of Staphylococcus aureus." *Mol. Microbiol.* 16(5): 895-907.

McDevitt, D., Nanavaty T., House-Pompeo K., Bell E., Turner N., McIntire L., Foster T., Hook M. (1997) "Characterization of the interaction between the Staphylococcus aureus clumping factor (ClfA) and fibrinogen." *Eur. J. Biochem.* 247(1): 416-24.

Meinders, J. M., van der Mei, H. C., Busscher, H.J., (1994) "Physicochemical aspects of deposition of Streptococcus thermophilus B to hydrophobic and hydrophilic substrata in a parallel plate flow chamber." *J. Colloid Interf. Sci.* 164: 355-363.

Merkel R., Nassoy P., Leung, A., Ritchie, K., Evans, E. (1999) "Energy landscapes of receptor-ligand bonds explored with dynamic force spectroscopy." *Nature* 397(7): 50-53.

Nylander, T. Wahlgren, N. M., (1997) "Forces between Adsorbed Layers of β-Casein." *Langmuir* 14(23): 6219-6225.

O'Grady, N., Alexander, M., Dellinger, E. P., Gerberding, J. L., Heard, S. O., Maki, D., Masur, H., McCormick, R. D., Mermel, L. A., Pearson, M. L., Raad, I .I., Randolph, A., M.D., Weinstein, R. A., (2002) "Guidelines for the prevention of intravascular catheter-related infections" *Morbidity and Mortality Weekly Report* 51(31): 1-29.

Olbrich, K. C., Andersen, T. T. , Blumenstock, F. A., Bizios, R. (1996) "Surfaces modified with covalently-immobilized adhesive peptides affect fibroblast population motility." *Biomaterials* 17(8): 759-764.

Ong, Y. L., Razatos, A., Georgiou, G., and Sharma, M. M. (1999) "Adhesion forces between E-coli bacteria and biomaterial surfaces." *Langmuir*, 15: 2719-2725.

Prieve, D. C., and Frej, N. A. (1990) "Total Internal Reflection Microscopy: A Quantitative Tool for the Measurement of Colloidal Forces." *Langmuir* 6: 396-403.

Prieve, D. C., Walz J. Y. (1993). "Scattering of an evanescent surface wave by a microscopic dielectric sphere." *Appl. Opt.* 32(9): 1629-1641.

Razatos, A., Ong, Y. L., Sharma, M. M., and Georgiou, G., (1998) "Evaluating the Interaction of Bacteria with Biomaterials using Atomic Force Microscopy." *J. Biomater. Sci. Polym. Ed.* 9:1361-1373.

Rijnaarts, H. H. M., Norde, W., Lyklema, J., Zehnder, A. J. B. (1999) "DLVO and steric contributions to bacterial deposition in media of different ionic strengths." *Colloids Surf., B* 14: 179-195.

Ruta, A. R. (1998). "Quantitative Study of Mechanisms of Bacterial Adhesion to Surfaces. Chemical Engineering." Thesis (Ph.D.)--University of Florida, Gainesville, FL.

Signas, C., Raucci, G., Jonsson, K., Lindgren, P.E., Anantharamaiah, G. M., Hook, M., Lindberg, M. (1989) "Nucleotide sequence of the gene for a fibronectin-binding protein from *Staphylococcus aureus:* use of this peptide sequence in the synthesis of biologically active peptides. *Proc. Natl. Acad. Sci. USA* 86:699-703.

Sjollema, J., Busscher, H. J., Weerkamp, A. H. (1990) "Real-time enumeration of adhering microorganisms in a parallel plate flow cell using automated image analysis." *J. Microbial Meth.* 9: 73-78.

Sokurenko, E. V. (1995) *Bacterial Adhesion Measured by Growth of Adherent Organisms. Methods in Enzymology*, 253: 519-529. Academic Press, Inc., New York.

Stephenson, J., Goldsmith, M. F. (2002) "CDC campaign targets antimicrobial resistance in hospitals." *JAMA*, 287(18): 2351-52.

Stewart, P. S., Costerton, J. W. (2001) "Antibiotic resistance of bacteria in biofilms." *Lancet* 358: 135-138.

Switalski, L.M., Speziale, P., and Hook, M. (1989) "Isolation and characterization of a putative collagen receptor from Staphylococcccus strain Cowan 1." *J. Biol. Chem.* 264: 21080-21086.

Torney, D. C., Dembo M. (1986) "Thermodynamics of cell adhesion. II. Freely mobile repellers." *Biophys J.* 49(2): 501-7.

Truesdail, S. E. (1999) "Fundamental forces important to the enhancement of biological colloid removal." Thesis (Ph.D.)--University of Florida, Gainesivlle, FL.

Uyen, H. M. W., Shaakenraad, J.M, Sjollema, J. (1990) "Amount and surface structure of albumin adsorbed to solid substrata with different wettabilities in a parallel plate flow cell." *J. Biomed. Mater. Res.* 24: 1599-1614.

van der Mei, H. C., Busscher, H. J., Bos, R., de Vries, J., Boonaert, C .J., and Dufrene, Y. F. (2000) "Direct probing by atomic force microscopy of the mechanical properties of a fibrillated and non-fibrillated oral streptococcal strain." *Biophys J.* 78, 2668-2674.

van der Wal, A., Minor, M., Zehnder, A. J. B., Lyklema, J. (1999) "Determination of total charge in the cell walls of gram positive bacteria." *Colloids Surf., B* 9: 81-100.

van Loosdrecht, M. C., Norde, W., and Zehnder, A. J., (1990) "Physical chemical description of bacterial adhesion." *J. Biomater. Appl.* 5: 91-97.

van Oss, C.J. (1995) Hydrophobicity of biosurfaces – origin, quantitative determination and interaction energies. *Colloids Surf., B* 5: 91-110

Vaudaux, P.E., Francois, P., Proctor, R. A., McDevitt, D., Foster, T .J., Albrecht, R. M., Lew, D. P., Wabers, H., and Cooper, S. L. (1995) "Use of adhesion-defective mutants of *Staphylococcus aureus* to define the role of specific plasma proteins in promoting bacterial adhesion to canine arterio-venous shunts." *Infect. Immun.* 63: 585-590.

Vaudaux, P., Pittet, D., Haeberli, A., Lerch, P.G., Morgenthaler, J.J., Proctor, R.A., Waldvogel, F.A., and Lew, D.P. (1993) "Fibronectin is more active than fibrin or fibrinogen in promoting Staphylococcus aureus adherence to intravascular devices." *J. Infect. Dis.* 167: 633-641.

Viani, M. B., Schaffer, T. E., Chand, A., Rief, M., Gaub, H. E., and Hansma, P. K. (1999) "Small cantilevers for force spectroscopy of single molecules." *J. Appl. Phys.* 86, 2258-2262.

Vogt, R. F. J., Phillips, D. L. (1987) "Quantitative differences among various proteins as blocking agents for ELISA microtiter plates." *J. Immunol. Methods* 101: 43-50.

Wit, P. J., Poortinga, A., Noordmans, J., van der Mei, H. C., Busscher, H. J. (1999) "Deposition of Polystyrene Particles in a Parallel Plate Flow Chamber under Attractive and Repulsive Attractive Conditions." *Langmuir* 18(8): 2620-2626.

Wong, S. S. (1993) *Chemistry of Protein Conjugation and Cross-Linking.* CRC Press, Inc., Boca Raton.

Yao, X., Walter J., Burke, S., Stewart, S., Jericho, M. H., Pink, D., Hunter, R., Beveridge, T. J. (2002) "Atomic force microscopy and theoretical considerations of surface properties and turgor pressures of bacteria" Pages 213-230 *Colloids Surf. B* 23: 213-230.

BIOGRAPHICAL SKETCH

Jonah David Klein was born on May 3, 1974 in Toledo Ohio. The son a university professor, Jonah lived in Albuquerque, New Mexico and Perth, Australia during his father's sabbatical leave from the University of Toledo. He attended Ottawa Hills High School in Toledo, Ohio and the University of Michigan, Ann Arbor where he received his Bachelor's of Science in Chemical Engineering. Prior to attending graduate school, Jonah was employed by BASF Corporation in Wyandotte Michigan, where he worked as a process engineer in a thermoplastic urethanes facility. Following admission to the University of Florida Department of Chemical Engineering in 1997, Jonah also earned a Master's Degree in Biomedical Engineering while conducting his Doctoral Research.

I certify that I have read this study and that in my opinion it conforms to acceptable standards of scholarly presentation and is fully adequate, in scope and quality, as a dissertation for the degree of Doctor of Philosophy.

Richard B. Dickinson, Chairman
Associate Professor of Chemical
Engineering

I certify that I have read this study and that in my opinion it conforms to acceptable standards of scholarly presentation and is fully adequate, in scope and quality, as a dissertation for the degree of Doctor of Philosophy.

Spyros A. Svoronos

Spyros A. Svoronos
Professor of Chemical Engineering

I certify that I have read this study and that in my opinion it conforms to acceptable standards of scholarly presentation and is fully adequate, in scope and quality, as a dissertation for the degree of Doctor of Philosophy.

Chang Won Park

Chang-Won Park
Professor of Chemical Engineering

I certify that I have read this study and that in my opinion it conforms to acceptable standards of scholarly presentation and is fully adequate, in scope and quality, as a dissertation for the degree of Doctor of Philosophy.

Anthony Bren

Anthony B. Brennan
Professor of Materials Science and
Engineering

This dissertation was submitted to the Graduate Faculty of the College of Engineering and to the Graduate School and was accepted as partial fulfillment of the requirements for the degree of Doctor of Philosophy.

December 2002

Pramod Khargonekar

Pramod P. Khargonekar
Dean, College of Engineering

Winfred M. Phillips
Dean, Graduate School